Oncogenic RAS Signalling Promotes Tumour Immunoresistance by Stabilising *PD-L1* mRNA

Matthew A. Coelho [1], Sophie de Carné Trécesson [1], Sareena Rana [7], Davide Zecchin [1], Christopher Moore [1], Miriam Molina-Arcas [1], Phil East [2], Bradley Spencer-Dene [3], Emma Nye [3], Karin Barnouin [4], Ambrosius P. Snijders [4], Wi S. Lai [5], Perry J. Blackshear [5,6] and Julian Downward [1,7,8,*]

[1] Oncogene Biology, [2] Computational Biology, [3] Experimental Histopathology and [4] Protein Analysis and Proteomics Laboratories,
The Francis Crick Institute, 1 Midland Road, London NW1 1AT, UK.

[5] Signal Transduction Laboratory, National Institute of Environmental Health Sciences, Research Triangle Park, North Carolina, USA.

[6] Departments of Medicine and Biochemistry, Duke University Medical Center, Durham, North Carolina, USA.

[7] Lung Cancer Group, Division of Molecular Pathology,
The Institute of Cancer Research, 237 Fulham Road, London SW3 6JB, UK.

[8]Lead Contact. *Correspondence: Julian.Downward@crick.ac.uk

Keywords

RAS; KRAS; immunotherapy; tristetraprolin; PD-L1

Summary

The immunosuppressive protein PD-L1 is upregulated in many cancers and contributes to evasion of the host immune system. The relative importance of the tumour microenvironment and cancer cell-intrinsic signalling in the regulation of PD-L1 expression remains unclear. We report that oncogenic RAS signalling is sufficient to upregulate tumour cell PD-L1 expression through a mechanism involving increases in *PD-L1* mRNA stability via modulation of the AU-rich element-binding protein tristetraprolin (TTP). TTP negatively regulates PD-L1 expression through AU-rich elements in the 3'UTR of *PD-L1* mRNA. MEK signalling downstream of RAS leads to MK2 induced phosphorylation and inhibition of TTP. In human lung and colorectal tumours, RAS pathway activation is associated with elevated PD-L1 expression. *In vivo*, restoration of TTP expression enhances anti-tumour immunity dependent on degradation of *PD-L1* mRNA. Our results demonstrate that RAS can drive cell-intrinsic PD-L1 expression, and present therapeutic opportunities to reverse the innately immunoresistant phenotype of *RAS* mutant cancers.

Highlights

- Oncogenic RAS signalling increases PD-L1 expression
- RAS regulates PD-L1 through AU-rich elements (AREs) in the 3'UTR of *PD-L1* mRNA
- The ARE-binding protein tristetraprolin (TTP) negatively regulates PD-L1 expression
- Restoration of tumour-cell TTP activity enhances anti-tumour immunity

eTOC Blurb

Coelho *et al*. demonstrate a post-transcriptional mechanism whereby oncogenic RAS signalling increases PD-L1 expression. Mechanistically, *PD-L1* mRNA is targeted by TTP through AU-rich elements in the 3'UTR, making it unstable. Oncogenic RAS signalling reduces TTP activity and stabilises the *PD-L1* transcript. Restoring TTP activity reduces PD-L1 levels and enhances anti-tumour immunity.

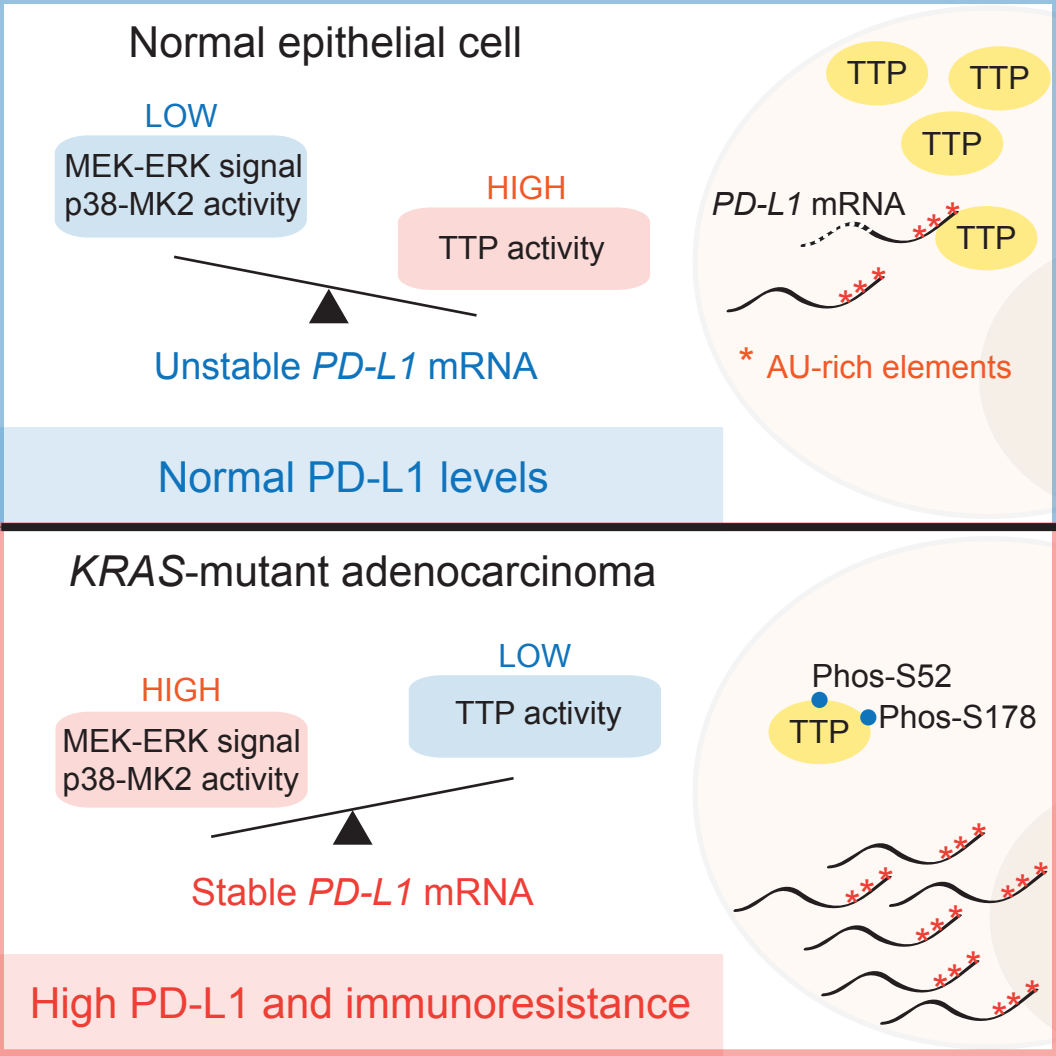
Normal epithelial cell
LOW
MEK-ERK signal
p38-MK2 activity
HIGH
TTP activity
Unstable PD-L1 mRNA
TTP
TTP
TTP
PD-L1 mRNA
TTP
* AU-rich elements
Normal PD-L1 levels
KRAS-mutant adenocarcinoma
HIGH
MEK-ERK signal
p38-MK2 activity
LOW
TTP activity
Stable PD-L1 mRNA
Phos-S52
TTP
Phos-S178
High PD-L1 and immunoresistance

Introduction

Therapeutic antibodies blocking PD-1 pathway activation by targeting PD-L1 (programmed death 1 ligand 1, also known as B7-H1 or CD274), or its receptor, PD-1, have caused striking regressions in several malignancies in which RAS mutations are frequent driver events, including non-small cell lung cancer (NSCLC) (Herbst et al., 2014; Topalian et al., 2012) and mismatch-repair-deficient colorectal cancer (Le et al., 2015). PD-L1 is critical for limiting autoimmune related damage to normal tissues in the context of chronic inflammation, but is also aberrantly upregulated on cancer cells in order to evade immune destruction (Pardoll, 2012). As anti-PD-1 pathway immunotherapies are only effective in a minority of cancer patients (Topalian et al., 2012), there is a great need for reliable biomarkers of patient response. To what degree tumour PD-L1 expression is prognostic of patient response to PD-1 pathway blockade remains contentious. Recent clinical trials of the anti-PD-1 antibody nivolumab report that tumour cell PD-L1 expression correlates with response to nivolumab in non-squamous, but not the squamous subtype of NSCLC (Borghaei et al., 2015; Brahmer et al., 2015). Notably, non-squamous NSCLC patients with *KRAS* mutations benefited from nivolumab therapy in terms of overall survival, whereas *KRAS* wild-type patients did not (Borghaei et al., 2015). Response rate and progression-free survival was increased in NSCLC patients treated with pembrolizumab in cases where at least 50 % of tumour cells were positive for PD-L1 (Garon et al., 2015). In this patient cohort, *KRAS* mutant tumours were more frequently PD-L1-positive than *KRAS* wild-type tumours.

The success of immune-checkpoint blockade is dependent on the immunogenicity of the tumour (Gubin et al., 2014; Linnemann et al., 2015; Rizvi et al., 2015), therefore one possible confounding factor in the use of tumour PD-L1 as a biomarker for response is the uncoupling of tumour PD-L1 expression from tumour immunogenicity. It is therefore critical to understand the signalling pathways that dictate tumour cell PD-L1 expression. The inflammatory cytokine IFN-γ is the best-characterized stimulus for PD-L1 expression, however, several studies suggest cell-intrinsic oncogenic signalling can also promote PD-L1 expression in cancer cells through EGFR, MYC and AKT (Akbay et al., 2013; Casey et al., 2016; Parsa et al., 2007). Studies performed on melanoma (Jiang et al., 2013) and acute myeloid leukaemia (Berthon et al., 2010) have indicated that MEK signalling is involved in upregulation of PD-L1 in some tumour cell lines, but the molecular basis of this regulation remains poorly defined.

Separately, genetic rearrangements in the 3'UTR of *PD-L1* have been found in a multitude of different cancers at low frequency, and are associated with massively increased levels of tumour *PD-L1* expression (Kataoka et al., 2016). These results imply that control of *PD-L1* expression through the 3'UTR might contribute to immune escape in human cancers, although the underlying mechanisms of post-transcriptional regulation responsible for this effect are unclear.

In this report, we reveal that tumour cell PD-L1 expression can be driven by oncogenic RAS pathway activation by a mechanism involving post-transcriptional regulation of the stability of *PD-L1* mRNA. This provides a

direct mechanism whereby RAS signalling in tumour cells can provide protection from attack by the immune system.

Results

Cell-intrinsic Upregulation of PD-L1 through Oncogenic RAS Signalling

We tested the potential role of oncogenic RAS signalling in the regulation of PD-L1 expression in human epithelial cells using ER-RAS^{G12V} fusion constructs, which allow for the induction of oncogenic RAS activity with 4-hydroxytamoxifen (4-OHT) (Molina-Arcas et al., 2013). As expected, addition of 4-OHT led to the rapid activation of oncogenic KRAS signalling through MEK and PI3K (Figure 1A) and coincided with induction of *c-MYC* and *CCND1* mRNA expression in an immortalised human pneumocyte cell line derived from type II cells (Figure 1B) (Kemp et al., 2008). *PD-L1* mRNA was rapidly increased following stimulation of oncogenic KRAS signalling with 4-OHT, resulting in a six-fold induction of mRNA expression after three hours (Figure 1B). By way of comparison with known regulators, stimulation with IFN-γ led to increases in *PD-L1* mRNA in excess of 10-fold after three hours and both KRAS activation and IFN-γ stimulation dramatically increased PD-L1 protein expression at the cell surface after 48 h (Figure 1C). Oncogenic HRAS signalling was also capable of inducing PD-L1 mRNA and protein expression in the immortalised breast epithelial cell line MCF10A, and the *KRAS* wild-type colon carcinoma cell line HKE-3 (Figure S1A and S1B), implying that induction of PD-L1 expression by RAS is not a tissue-specific or RAS-isoform specific phenomenon. The induction of PD-L1 protein was most striking in ER-HRAS^{G12V} MCF10A cells, perhaps reflecting the low basal levels of PD-L1 expression. Chronic RAS activation for four days led to more profound

increases in PD-L1 protein, whereas shorter-term activation resulted in modest inductions of PD-L1 expression (Figure S1B). Importantly, 4-OHT did not induce PD-L1 expression in parental cell lines lacking ER-RAS constructs (Figure S1C).

Direct inhibition of KRAS signalling with the $KRAS^{G12C}$-specific inhibitor ARS853 (Lito et al., 2016; Patricelli et al., 2016) in lung and colorectal cancer cell lines harbouring $KRAS^{G12C}$ mutations led to reductions in *PD-L1* mRNA expression, but not in the $KRAS^{G12S}$ A549 control lung cancer cell line (Figure 1D and 1E). Moreover, ARS853 treatment led to significant reductions in PD-L1 surface protein expression in the *KRAS*-mutant lung cancer cell line H358 (Figure 1F). To dissect which downstream effectors of RAS are responsible for regulating PD-L1 expression, we used the specific inhibitors of MEK and pan type I PI3Ks, GSK1120212 (trametinib) and GDC-0941 (pictilisib), respectively (Figure S1D). Notably, MEK and PI3K inhibitors could block RAS-induced expression of PD-L1 protein in ER-$KRAS^{G12V}$ type II pneumocytes, either alone, or in combination (Figure 1G). MEK inhibition significantly reversed KRAS-mediated *PD-L1* mRNA upregulation (Figure 1H), however PI3K inhibition only reduced PD-L1 protein expression, concordant with evidence for AKT signalling increasing PD-L1 expression predominantly through activating translation of the transcript (Parsa et al., 2007). MEK inhibition, but not PI3K inhibition, reduced *PD-L1* mRNA expression in H358 (Figure 1I), H23, and H1792 lung cancer cell lines (Figure S1E). Downstream of MEK, inhibition of ERK1/2 with SCH772984 potently reduced *PD-L1* expression in H358 and H23 cells (Figure S1F). Furthermore, PMA, a potent

chemical activator of MEK-ERK signalling via protein kinase C stimulation, dramatically and rapidly increased PD-L1 expression; an effect that was largely reversed with the inhibition of MEK (Figure 1J and Figure S1G). More extensive analysis of PD-L1 surface expression on multiple *KRAS*-mutant lung cancer cell lines, both human and murine, revealed generally consistent PD-L1 downregulation following MEK and PI3K inhibition, suggesting this regulatory pathway is of broad significance (Figure S1H). Taken together, these results suggest that oncogenic RAS signalling through MEK and PI3K is sufficient to drive PD-L1 expression.

Since RAS signalling has been implicated in reducing the expression of genes involved in the presentation of antigens by MHC class I molecules (Ebert et al., 2016; El-Jawhari et al., 2014), we analysed the expression of antigen processing and antigen presentation machinery following oncogenic RAS activation (Figure S1I). As expected, KRAS G12V signalling led to significant decreases in expression of *TAP1, TAPBP,* as well as *HLA-A*, *HLA-B*, *HLA-C* and *B2M*, suggesting that compromised antigen processing and presentation in concert with increases in PD-L1 expression may contribute to an augmented state of immunoresistance in *RAS*-mutant tumour cells.

RAS Signalling Increases *PD-L1* mRNA Stability through AU-rich Elements in the 3'UTR

To investigate how RAS-MEK signalling regulates PD-L1 expression, we first asked whether RAS regulates PD-L1 via a transcriptional mechanism. We generated a series of luciferase reporter constructs containing promoter

fragments cloned from the human *PD-L1* locus (Figure S2A). In all cases, the physiological stimulus IFN-γ, but not PMA, induced expression of the promoter reporter constructs in H358 cells, a cell line in which endogenous *PD-L1* mRNA expression is robustly induced with PMA (Figure 1J). Incorporation of putative enhancer elements (Sumimoto et al., 2016) into the PD-L1 promoter reporter constructs also failed to confer sensitivity to MAPK activation (Figure S2A), as did including predicted regulatory regions spanning the 5' of exon 1 (data not shown). Furthermore, none of the reporters showed evidence of decreased expression when H358 cells were treated with MEK inhibitor (data not shown).

Therefore, we investigated possible mechanisms of post-transcriptional regulation of PD-L1 expression by RAS. We induced oncogenic KRAS signalling with 4-OHT in ER-KRAS^{G12V} type II pneumocytes and concomitantly blocked transcription with actinomycin D. Surprisingly, we found human *PD-L1* mRNA to have a short half-life, which was significantly stabilised by the induction of oncogenic KRAS signalling (Figure 2A). Moreover, murine *PD-L1* mRNA also had a comparably short half-life, and the stability of the transcript in a *Kras*-mutant, p53-deleted murine lung tumour cell line (KPB6) could be reduced further still when MEK was inhibited (Figure 2B), implicating KRAS-MEK signalling in the stabilisation of the labile *PD-L1* transcript. Consistently, direct inhibition of oncogenic KRAS signalling with ARS853 also caused reductions in *PD-L1* mRNA half-life in H23, H1792 and H358 cells (Figure 2C). However, inhibition of PI3K alone did not result in altered *PD-L1* mRNA stability in KPB6 cells (Figure S2B).

Common genetic elements conferring mRNA instability include miRNA binding sites and AU-rich elements (AREs) in the 3'UTR of the transcript. The core motif for AREs is an ATTTA pentamer sequence, however functional AREs are often found in an AU-rich context, conforming to the WWATTTAWW nonamer consensus (where W denotes an A or T) (Zubiaga et al., 1995) constituting the binding site for several AU-rich element binding proteins (AUBPs), which can subsequently recruit mRNA decay machinery (Lykke-Andersen and Wagner, 2005). For example, a canonical ARE-regulated transcript is *TNF-α*, which contains nine pentamer sequences in the human transcript, and eight pentamers in the murine transcript. Upon inspection of the 3'UTR of *PD-L1*, we noted a high number of ARE pentamers. Specifically, out of 14 ATTTA pentamer sequences in the human transcript and 11 in the murine transcript, there were three conserved AREs conforming to the nonamer consensus (Figure 2D).

We tested the influence of MEK inhibition on the half-life of another unstable mRNA, *Tusc2* (tumour suppressor candidate 2, or *Fus1*), which does not contain AU-rich elements in the 3'UTR, but is targeted by multiple miRNAs (Du et al., 2009). Although *Tusc2* mRNA had a similar half-life to *PD-L1* mRNA, MEK inhibition did not influence the stability of the *Tusc2* transcript (Figure S2C), indicating that the observed post-transcriptional regulation of *PD-L1* by MEK may relate to AU-rich elements in the *3'UTR*. Indeed, a transcript containing functional AU-rich elements, *Ptgs2* mRNA (Cha et al., 2011) displayed a significant reduction in mRNA half-life in response to MEK inhibition (Figure S2C), reminiscent of *PD-L1* mRNA.

To directly analyse the functional importance of these AREs, we constructed a luciferase reporter containing a fragment of the 3'UTR of human *PD-L1* containing the last six ATTTA pentamers, including the three conserved nonamer sequences. Mutation of ATTTA pentamers to ATGTA has been shown to increase the expression of ARE-containing mRNAs (Rajagopalan et al., 1995; Yang et al., 2004). Consistent with this, mutating the six ATTTA pentamer sequences to ATGTA increased expression of the *PD-L1 3'UTR* luciferase reporter in ER-HRAS^{G12V} MCF10A and H358 cells, suggesting these AREs are functionally relevant for controlling the expression of PD-L1 (Figure 2E and 2F). Stimulation with 4-OHT in ER-HRAS^{G12V} MCF10A cells, or PMA in H358 cells, increased expression of the wild-type reporter, whereas the ATGTA mutant reporter was insensitive to these treatments (Figure 2E and 2F). In sum, these data suggest that AREs in the 3'UTR of *PD-L1* mRNA can mediate control of PD-L1 expression by RAS-MEK signalling.

AU-rich element Binding Proteins TTP and KSRP are Negative Regulators of PD-L1 Expression

To assess which AU-rich element binding proteins (AUBPs) could mediate regulation of PD-L1 expression downstream of RAS signalling, we performed a selected siRNA screen of likely candidate genes: *AUF1*, *KSRP*, *HuR* and *TTP* (also known as tristetraprolin or *ZFP36*), in three *RAS*-mutant lung cancer cell lines (Figure 3A-C). Knockdown efficiency was verified in each case by qPCR (Figure S3A-C). siRNA-mediated knockdown of *KSRP*

and *TTP* most consistently increased *PD-L1* mRNA expression across the cell line panel, with the exception A427 where knock-down of *TTP* did not lead to significantly increases in *PD-L1* mRNA levels. Overexpression of KSRP or TTP was sufficient to significantly decrease *PD-L1* expression (Figure 3D) and *PD-L1 3'UTR* luciferase reporter expression in H358 cells (Figure 3E), corroborating our results from the siRNA screen and confirming that KSRP and TTP impart their negative regulation of PD-L1 expression through the 3'UTR. Overexpression of TTP and KSRP together did not result in additive reductions in PD-L1 expression, suggesting that they may regulate PD-L1 through the same mechanism (Figure S3D). Notably, siRNA-mediated knockdown of TTP family members, BRF-1 and BRF-2, was incapable of increasing *PD-L1* expression to the extent achieved by silencing TTP expression (Figure S3E and S3F). We confirmed that TTP protein expression was reduced following knock-down in H23 and H358 cells, but this was less clear in A427 cells, which express lower levels of TTP protein (Figure S3G). Deconvolution of siRNA pools targeting *TTP* showed that multiple siRNAs increased expression of *PD-L1* mRNA in H23 and H358 cells (Figure S3H).

We further examined the regulation of *PD-L1* mRNA by TTP by using TTP wild-type (WT) and TTP knock-out (KO) MEFs. In the TTP KO MEFs, *TTP* mRNA is expressed but no functional TTP protein can be made due to the introduction of a premature stop codon at the endogenous locus (Lai et al., 2006; Taylor et al., 1996). Acute activation of *TTP* expression with serum temporally coincided with a dramatic and transient decrease in *PD-L1* mRNA in TTP WT MEFs, but not in the TTP KO MEFs (Figure 3F), with *PD-L1* levels

recovering to near baseline at six hours after serum addition. Moreover, the total absence of functional TTP protein in the TTP KO MEFs increased the half-life of *PD-L1* mRNA relative to TTP WT MEFs (Figure 3G).

Finally, we generated a KPB6 lung cancer cell line with a tetracycline-inducible TTP transgene (TTP tet-ON). As expected, inducible expression of TTP led to reductions in wild-type *PD-L1* 3'UTR luciferase reporter expression, but not of the ATGTA mutant 3'UTR reporter (Figure 3H). When combined with MEK inhibition, TTP expression more robustly suppressed expression of the wild-type reporter. In sum, these data provide evidence for the negative regulation of *PD-L1* mRNA expression by the AUBPs KSRP and TTP.

RAS Regulates PD-L1 Expression through TTP

To further investigate whether MEK and TTP regulate PD-L1 via a shared pathway, we silenced *TTP* expression using siRNAs in the context of MEK inhibition. Knock-down of *TTP* was largely able to rescue the decrease in *PD-L1* expression caused by MEK inhibition (Figure 4A). However, the knockdown of *KSRP* could not rescue this phenotype, despite profound silencing of expression (Figure S4A). Furthermore, MEK inhibition significantly increased *TTP* mRNA expression (Figure 4A), and chronic activation of oncogenic KRAS signalling significantly decreased *TTP* mRNA expression (Figure 4B).

Next, we tested whether the RAS pathway regulates the activity of TTP and/or KSRP protein. Crucially, we found that endogenous levels of TTP and

KSRP both co-precipitated with *PD-L1* mRNA in RNA immunoprecipitation (RNA-IP) reactions from KPB6 mouse lung cancer cells (Figure S4B). TTP also significantly bound to *PD-L1* mRNA in H358 cells (Figure 4C). In all cases, the enrichment for the *PD-L1* transcript was far greater than that of a control mRNA, *GAPDH*, which lacks AREs in the 3'UTR (Figure 4C, Fig S4C). MEK inhibition did not significantly alter the occupancy of TTP or KSRP on *PD-L1* mRNA, consistent with RAS regulating the activity of the AUBP, rather than the occupancy on the target mRNA.

ERK has been shown to phosphorylate (Taylor et al., 1995) and negatively regulate TTP activity and expression (Bourcier et al., 2011; Deleault et al., 2008; Essafi-Benkhadir et al., 2007; Hardle et al., 2015). Inhibition of MEK decreased phosphorylation of TTP at PXSP (ERK target-site consensus) and RXXS/T (RSK/AKT target-site consensus) motifs (Figure 4D and 4E), confirming that TTP is regulated by phosphorylation downstream of MEK signalling in cancer cells. Mutation of two of the highest confidence predicted ERK-target residues on human TTP (S218 and S228) abrogated detection of TTP with the phospho-PXSP motif-specific antibody (Figure 4D), however the phosphosite-mutant TTP (S218A 228A) did not show enhanced activity in reducing *PD-L1* mRNA expression compared to wild-type TTP (data not shown), implying the involvement of other residues that are not readily detected with this antibody. Furthermore, although AKT signalling has been shown to regulate KSRP activity through phosphorylation of S193 (Diaz-Moreno et al., 2009), the KSRP S193A phosphosite-mutant did not show

enhanced activity in reducing *PD-L1* mRNA expression compared to wild-type KSRP (Figure S4D).

Equally, the serine/threonine phosphatase PP2A has been implicated in positively regulating TTP function by reversing inhibitory phosphorylation events (Sun et al., 2007). Therefore, we tested whether inhibition of PP2A with okadaic acid (OA) would increase PD-L1 expression. OA rapidly increased *PD-L1* mRNA expression in TTP WT MEFs, but not TTP KO MEFs (Figure 4F), demonstrating that PP2A activity decreases PD-L1 expression specifically through modulating TTP activity.

RAS-ROS-p38 Signalling Controls TTP Activity

To discover which residues are functionally important for regulating TTP activity downstream of RAS, we performed mass spectrometry on immunoprecipitated Myc-TTP after PMA, MEK inhibitor, or PMA and MEK inhibitor treatment. We used the *Kras*-mutant, mouse colon carcinoma cell line CT26, based on its immunogenicity and sensitivity to anti-PD-L1 antibody therapy, making it suitable for downstream *in vivo* experiments. Most notably, mass spectrometry analysis revealed MEK-dependent phosphorylation of S52 and S178; PMA significantly enhanced phosphorylation of these residues, and this effect was reversed with MEK inhibition (Figure 5A, S5A and Table S1). Moreover, MEK inhibition alone was sufficient to reduce phosphorylation of these residues (Figure 5A).

S52 and S178 residues are crucial for the regulation of TTP activity through binding to 14-3-3 proteins following phosphorylation by MK2 (also

known as MAPKAPK2) downstream of p38 (Chrestensen et al., 2004). Consequently, p38 signalling results in decreased TTP activity, partly through reducing the association with deadenylase machinery (Mahtani et al., 2001; Stoecklin et al., 2004). In parallel, phosphorylation of S52 and S178 stabilises TTP protein (Brook et al., 2006), which is consistent with the observed increase in abundance of total TTP peptides detected in the PMA versus the MEK inhibitor-treated condition (Figure 5A).

We reasoned that oncogenic RAS might stimulate p38 signalling through promoting the MEK-dependent accumulation of reactive oxygen species (ROS) (Nicke et al., 2005), and thus inhibit TTP function. Indeed, oncogenic RAS signalling dramatically increased intracellular ROS in MCF10A cells, and ROS levels were distinctly correlated with the extent of PD-L1 induction (Figure S5B). Furthermore, the addition of the potent anti-oxidant N-acetyl-L-cysteine (NAC) largely reversed the induction of PD-L1 protein by RAS (Figure 5B and Figure S5B), collectively suggesting that ROS induction by oncogenic RAS is functionally important in driving PD-L1 expression.

Specific activation of the p38 pathway using an inducible version of the upstream kinase MEKK3 (ΔMEKK3-ER) (Figure 5C and Figure S5C) (Garner et al., 2002) was sufficient to increase PD-L1 protein expression, albeit to a lesser extent than that achieved by RAS itself. Co-treatment with NAC was considerably less effective in reversing PD-L1 induction in this context, consistent with ROS operating upstream of p38 in this pathway (Figure 5C). Moreover, inhibition of MK2 strongly reversed RAS-induced PD-L1 expression in MCF10A and HKE-3 cells (Figure 5D) and PD-L1 expression in CT26 cells,

which have endogenous levels of mutant Kras (Figure 5E). We also observed reductions in expression of *PD-L1* mRNA in several NSCLC cell lines with endogenous *KRAS* mutations following treatment with NAC, reduced glutathione or MK2 inhibitor III (Figure S5D), although we noted some heterogeneity in response between the four cell lines tested.

To directly test the functional significance of the MK2 target residues downstream of MEK pathway activation, we generated TTP knock-out CT26 cell lines using CRISPR-Cas (to obviate functional contributions from endogenous TTP), and reconstituted these cells with either a wild-type (WT) or phosphosite-mutant (S52A S178A), tetracycline-inducible TTP transgene. S52 and S178 of mouse TTP are highly conserved, with S52 conforming to the RXXS/T phosphosite motif (Figure 5F). Immunoprecipitation of Myc-tagged TTP following acute MAPK activation with PMA revealed phosphorylation of WT TTP, but not of the S52A S178A mutant protein at RXXS/T sites (Figure 5G), verifying our findings from mass spectrometry analysis. Crucially, the S52A S178A mutant TTP had significantly enhanced activity in reducing *PD-L1* mRNA expression relative to WT TTP (Figure 5H and Figure S5E). In sum, these results suggest that a RAS-ROS-p38 signalling axis contributes to PD-L1 upregulation through phosphorylation and inactivation of TTP.

RAS Pathway Activation is Associated with PD-L1 Upregulation in Human Cancers

To further evaluate the role of oncogenic RAS signalling in regulating PD-L1 expression in cancer, we analysed TCGA gene expression data from patient-derived lung adenocarcinoma (LUAD) or colon adenocarcinoma (COAD) samples. To account for the effects of alternative oncogenes that can activate downstream RAS effector pathways such as EGFR, BRAF and ALK, we used two published gene expression signatures for RAS activation (Loboda et al., 2010; Sweet-Cordero et al., 2005) to segregate patient samples into “high” and “low” RAS pathway activity based on gene expression. As expected, annotation of *KRAS* mutation status revealed a strong enrichment for *KRAS* mutant samples in the high RAS activity cohorts in both signatures (Figure 6A and S6A). We compared the expression of T cell function related genes between high and low RAS activity cohorts and found *CD274* (*PD-L1*) expression to be significantly increased in the high RAS pathway activity samples in LUAD (1.42 log2-fold change) and COAD samples (1.17 log2-fold change), using either signature (Figure 6A, 6B and S6A). Stromal PD-L1 and tumour PD-L1 expression appear to have independent, suppressive effects on anti-tumour immunity (Lau et al., 2017), however we noted that the expression of the pan-leukocyte marker *PTPRC* (coding for CD45) and lymphocyte marker *CD3E*, were only modestly increased in the high RAS pathway activity cohort, indicating that the differential in *PD-L1* expression is not likely to be solely attributable to a higher degree of leukocyte infiltration in the tumour microenvironment (Figure 6A).

Of note, *IFNGR1* was also among the most significantly enriched transcripts in the high RAS pathway activity groups. To investigate the possibility that PD-L1 may be upregulated in RAS active tumours due to regulation by IFNGR1, we induced PD-L1 expression with RAS in ER-KRAS^{G12V} type II pneumocytes and concomitantly blocked IFNGR1 signalling using a depleting antibody for IFN-γ, or with the JAK1/2 inhibitor ruxolitinib. Although both treatments effectively reduced responses to exogenous IFN-γ, PD-L1 induction by RAS was unaffected, suggesting independence from IFN-γ-IFNGR1 signalling (Figure 6SB).

To further explore the *in vivo* relevance of TTP regulation in human cancer, we compared *TTP* expression in normal tissue and tumour samples by using publically available datasets. *TTP* expression was strikingly downregulated in human lung and colon tumour samples compared to normal tissue (Selamat et al., 2012; Skrzypczak et al., 2010) (Figure S6C), confirming that aberrant regulation of *TTP* expression is relevant in the human disease. Consistently, in FACS-sorted epithelial cells isolated from normal lung or matched tumour tissue from *Kras*$^{LSL\text{-}G12D/+}$; *Trp53*$^{F/F}$ (KP) mice, *TTP* expression was reduced in lung tumour tissue (Figure S6D). *PD-L1* mRNA expression was generally higher in tumour tissue than in normal lung but not significantly increased, however, PD-L1 protein expression was significantly elevated, perhaps reflecting the contribution from AKT in promoting PD-L1 protein expression (Figure S6E).

Restoration of Tumour Cell TTP Expression Enhances Anti-tumour Immunity

Next, we set out to directly assess the functional importance of the regulation of PD-L1 expression by TTP in tumour progression. To this end, we generated a series of stable CT26 cell lines expressing Myc-tagged, mouse TTP under a tetracycline-inducible promoter (TTP tet-ON), and in addition, constitutively expressing either empty vector, or mouse *PD-L1* cDNA lacking the 3'UTR (PD-L1 Δ3'UTR). TTP expression was induced upon addition of doxycycline in a dose-dependent manner (Figure 7A), resulting in decreased PD-L1 protein expression at the cell surface (Figure 7B). Overexpression of PD-L1 Δ3'UTR rendered total PD-L1 levels effectively insensitive to TTP induction (Figure 7B). TTP transgene expression with doxycycline was also associated with a decrease in *PD-L1* mRNA stability, which was comparable to that mediated by MEK inhibition in this system (Figure S7A).

To independently verify our findings in another cell line, we used MC38 tumour cells because they are known to exhibit sensitivity to PD-L1 modulation *in vivo*, and show Ras pathway activation (Giannou et al., 2017). As expected, TTP was induced with doxycycline in MC38 (tet-ON) cells, leading to reductions in PD-L1 expression (Figure S7B and S7C).

Using these engineered cell lines, we performed subcutaneous transplantation experiments in mice and monitored tumour progression. Notably, the growth rates of the stable cell lines *in vitro* did not significantly differ with the overexpression of PD-L1 Δ3'UTR cDNA or the induction of TTP transgene expression with doxycycline (Figure S7D and S7E). However, *in*

vivo, doxycycline treatment significantly reduced CT26 and MC38 tumour growth in immune competent, syngeneic mice (Figure 7C and 7D). Strikingly, the anti-tumour effects mediated by doxycycline treatment were absent in immunocompromised *nu/nu* mice harbouring CT26 tumours (Figure 7E), and in mice treated with depleting antibodies against CD8 and CD4, implying an essential contribution from the adaptive immune system to this anti-tumour response (Figure 7F). CT26 tumour cells overexpressing PD-L1 Δ3'UTR grew faster than the empty vector cells in BALB/c mice, but had no growth advantage in *nu/nu* mice. Moreover, expression of PD-L1 Δ3'UTR was able to rescue much of the growth inhibition mediated by doxycycline treatment in BALB/c mice, suggesting that suppression of tumour cell PD-L1 expression is an essential component of the anti-tumour effects mediated by TTP transgene induction (Figure 7C). As expected, CT26 cells expressing a PD-L1 cDNA with the full-length, wild-type 3'UTR had considerably lower expression of PD-L1 protein than the PD-L1 Δ3'UTR cells, but still responded to TTP induction in terms of reductions in PD-L1 expression (Figure S7F) and control of tumour growth in immune competent mice (Figure S7G).

Consistent with a heightened anti-tumour immune response, tumours derived from mice treated with doxycycline had a greater degree of $CD3^+$ lymphocyte infiltration than tumours from mice treated with vehicle, and this corresponding infiltration was abrogated in tumours derived from cells overexpressing PD-L1 Δ3'UTR (Figure 7G and Figure S7H). Moreover, we found higher $CD8^+$/Treg ratios in tumours expressing the TTP transgene, and higher levels of IFN-γ production by $CD8^+$ tumour-infiltrating lymphocytes

(TILs) derived from TTP-expressing tumours, versus PD-L1 Δ3'UTR tumours expressing TTP (Figure 7H), however we did not find significant differences in $CD4^+$ TIL populations (data not shown).

Collectively, these data highlight the functional importance of the regulation of PD-L1 expression by TTP in tumour progression, and demonstrate that this novel regulatory pathway may be exploited for the treatment of *Ras*-mutant cancers. These findings support a model whereby tumour-specific suppression of TTP can foster PD-L1 upregulation, and ultimately, tumour immunoresistance (Figure 7I and Figure S7I).

Discussion

In this report, we demonstrate that oncogenic RAS signalling can increase tumour cell-intrinsic PD-L1 expression, implying that mutant RAS oncogenes can directly contribute to the evasion of immune destruction in cancer. We reveal that RAS-MEK signalling controls expression of PD-L1, at least in part, by modulating the stability of the transcript. We show that the mouse and human *PD-L1* mRNAs are labile transcripts containing functional AU-rich elements (AREs) in the 3'UTR that permit regulation of PD-L1 expression by RAS. Crucially, our data provide a potential explanation for the genomic structural variations in the *PD-L1* 3'UTR observed in human cancer (Kataoka et al., 2016). The simultaneous loss of regulation by miRNAs and AREs is likely to contribute to the high levels of overexpression observed in tumours with complete loss of the 3'UTR. In addition, we provide a molecular basis for the tendency of *KRAS*-mutant NSCLCs to be positive for PD-L1 expression (D'Incecco et al., 2015; Dong et al., 2017; Li et al., 2017; Yang et al., 2017), implying that PD-1/PD-L1 blockade may prove more successful in *RAS*-mutant patients that also harbour a sufficient number of tumour-antigens.

We identify TTP as a principle AU-rich element binding protein responsible for negatively regulating PD-L1 expression, consistent with a previous report identifying *PD-L1* mRNA as one of a number of TTP targets in an RNA-immunoprecipitation, microarray-based screen in mouse macrophages (Stoecklin et al., 2008). Mechanistically, MEK inhibition reduced *PD-L1* mRNA stability, coinciding with an increase in TTP expression and reduction in phosphorylation of TTP at ERK and RSK/AKT consensus motifs.

Conversely, activation of RAS and the associated ROS accumulation led to enhanced TTP phosphorylation, notably by MK2 at key inhibitory sites.

TTP transgene expression restrained tumour growth in CT26 and MC38 tumour transplantation models. This anti-tumour effect is predominantly non-cell autonomous, dependent on the adaptive immune system and suppression of tumour cell PD-L1 expression. We noted only minor reductions in tumour growth rates following TTP transgene induction in cells overexpressing PD-L1 Δ3'UTR. TTP has been reported to have cell-autonomous tumour suppressive roles (Rounbehler et al., 2012) and non-cell autonomous anti-tumour effects through targeting VEGF and COX-2 mRNAs (Cha et al., 2011; Essafi-Benkhadir et al., 2007), which may contribute to some of these ostensibly PD-L1-independent effects, the magnitude of which are likely to be determined by the level of TTP overexpression in each system.

Our data extend the molecular understanding of the regulation of PD-L1 expression in cancer and highlight druggable targets to enhance anti-tumour immunity in tumours that are wild type for *PD-L1 3'UTR*. We provide evidence that pharmacological targeting of RAS, or RAS effector proteins, may elicit non-cell autonomous anti-tumour effects in *RAS*-mutant tumours. Recently, MEK inhibitors and PD-1 pathway blockade were shown to combine strongly in a mouse model of *Ras*-mutant colon carcinoma (Ebert et al., 2016; Liu et al., 2015). We anticipate that our findings will inform the development of effective combination therapies with immune checkpoint blockade in cancer.

Supplemental Information

Supplemental Information, including seven supplemental figures and two supplemental tables, can be found with this article online.

Author Contributions

M.A.C and J.D designed the study, interpreted the results and wrote the manuscript. M.A.C, S.C.T and S.R performed the biochemical experiments, D.Z and C.M assisted with *in vivo* studies, B.S.D and E.N performed histopathological studies, S.C.T and P.E performed bioinformatics analyses, K.B and A.P.S performed mass spectrometry analyses and W.S.L and P.J.B provided TTP KO and WT MEFs. All authors contributed to manuscript revision and review.

Acknowledgements

We thank Charles Swanton and Caetano Reis e Sousa for helpful, David Hancock and Febe Van Maldegem for critical reading of the manuscript and science technology platforms at the Francis Crick Institute including Biological Resources, FACS, Equipment Park, Experimental Histopathology and Cell Services. We thank Lynn McGregor and Kevan Shokat for providing ARS853. This work was supported by the Francis Crick Institute, which receives its core funding from Cancer Research UK (FC001070), the UK Medical Research Council (FC001070), and the Wellcome Trust (FC001070), and by funding from the European Research Council Advanced Grant RASTARGET and a Wellcome Trust Senior Investigator Award 103799/Z/14/Z.

References

Akbay, E.A., Koyama, S., Carretero, J., Altabef, A., Tchaicha, J.H., Christensen, C.L., Mikse, O.R., Cherniack, A.D., Beauchamp, E.M., Pugh, T.J.*, et al.* (2013). Activation of the PD-1 Pathway Contributes to Immune Escape in EGFR-Driven Lung Tumors. Cancer discovery *3*, 1355-1363.

Berthon, C., Driss, V., Liu, J.Z., Kuranda, K., Leleu, X., Jouy, N., Hetuin, D., and Quesnel, B. (2010). In acute myeloid leukemia, B7-H1 (PD-L1) protection of blasts from cytotoxic T cells is induced by TLR ligands and interferon-gamma and can be reversed using MEK inhibitors. Cancer Immunol Immun *59*, 1839-1849.

Borghaei, H., Paz-Ares, L., Horn, L., Spigel, D.R., Steins, M., Ready, N.E., Chow, L.Q., Vokes, E.E., Felip, E., Holgado, E.*, et al.* (2015). Nivolumab versus Docetaxel in Advanced Nonsquamous Non-Small-Cell Lung Cancer. New Engl J Med *373*, 1627-1639.

Bourcier, C., Griseri, P., Grepin, R., Bertolotto, C., Mazure, N., and Pages, G. (2011). Constitutive ERK activity induces downregulation of tristetraprolin, a major protein controlling interleukin8/CXCL8 mRNA stability in melanoma cells. American journal of physiology. Cell physiology *301*, C609-618.

Brahmer, J., Reckamp, K.L., Baas, P., Crino, L., Eberhardt, W.E., Poddubskaya, E., Antonia, S., Pluzanski, A., Vokes, E.E., Holgado, E.*, et al.* (2015). Nivolumab versus Docetaxel in Advanced Squamous-Cell Non-Small-Cell Lung Cancer. The New England journal of medicine *373*, 123-135.

Brook, M., Tchen, C.R., Santalucia, T., McIlrath, J., Arthur, J.S., Saklatvala, J., and Clark, A.R. (2006). Posttranslational regulation of tristetraprolin subcellular localization and protein stability by p38 mitogen-activated protein kinase and extracellular signal-regulated kinase pathways. Molecular and cellular biology *26*, 2408-2418.

Casey, S.C., Tong, L., Li, Y., Do, R., Walz, S., Fitzgerald, K.N., Gouw, A.M., Baylot, V., Gutgemann, I., Eilers, M., and Felsher, D.W. (2016). MYC regulates the antitumor immune response through CD47 and PD-L1. Science *352*, 227-231.

Cha, H.J., Lee, H.H., Chae, S.W., Cho, W.J., Kim, Y.M., Choi, H.J., Choi, D.H., Jung, S.W., Min, Y.J., Lee, B.J.*, et al.* (2011). Tristetraprolin downregulates the expression of both VEGF and COX-2 in human colon cancer. Hepatogastroenterology *58*, 790-795.

Chrestensen, C.A., Schroeder, M.J., Shabanowitz, J., Hunt, D.F., Pelo, J.W., Worthington, M.T., and Sturgill, T.W. (2004). MAPKAP kinase 2 phosphorylates tristetraprolin on in vivo sites including Ser178, a site required for 14-3-3 binding. The Journal of biological chemistry *279*, 10176-10184.

D'Incecco, A., Andreozzi, M., Ludovini, V., Rossi, E., Capodanno, A., Landi, L., Tibaldi, C., Minuti, G., Salvini, J., Coppi, E.*, et al.* (2015). PD-1 and PD-L1 expression in molecularly selected non-small-cell lung cancer patients. Br J Cancer *112*, 95-102.

Deleault, K.M., Skinner, S.J., and Brooks, S.A. (2008). Tristetraprolin regulates TNF TNF-alpha mRNA stability via a proteasome dependent

mechanism involving the combined action of the ERK and p38 pathways. Mol Immunol *45*, 13-24.

Diaz-Moreno, I., Hollingworth, D., Frenkiel, T.A., Kelly, G., Martin, S., Howell, S., Garcia-Mayoral, M., Gherzi, R., Briata, P., and Ramos, A. (2009). Phosphorylation-mediated unfolding of a KH domain regulates KSRP localization via 14-3-3 binding. Nat Struct Mol Biol *16*, 238-246.

Dong, Z.Y., Zhong, W.Z., Zhang, X.C., Su, J., Xie, Z., Liu, S.Y., Tu, H.Y., Chen, H.J., Sun, Y.L., Zhou, Q.*, et al.* (2017). Potential Predictive Value of TP53 and KRAS Mutation Status for Response to PD-1 Blockade Immunotherapy in Lung Adenocarcinoma. Clin Cancer Res *23*, 3012-3024.

Du, L., Schageman, J.J., Subauste, M.C., Saber, B., Hammond, S.M., Prudkin, L., Wistuba, II, Ji, L., Roth, J.A., Minna, J.D., and Pertsemlidis, A. (2009). miR-93, miR-98, and miR-197 regulate expression of tumor suppressor gene FUS1. Mol Cancer Res *7*, 1234-1243.

Ebert, P.J., Cheung, J., Yang, Y., McNamara, E., Hong, R., Moskalenko, M., Gould, S.E., Maecker, H., Irving, B.A., Kim, J.M.*, et al.* (2016). MAP Kinase Inhibition Promotes T Cell and Anti-tumor Activity in Combination with PD-L1 Checkpoint Blockade. Immunity *44*, 609-621.

El-Jawhari, J.J., El-Sherbiny, Y.M., Scott, G.B., Morgan, R.S., Prestwich, R., Bowles, P.A., Blair, G.E., Tanaka, T., Rabbitts, T.H., Meade, J.L., and Cook, G.P. (2014). Blocking oncogenic RAS enhances tumour cell surface MHC class I expression but does not alter susceptibility to cytotoxic lymphocytes. Mol Immunol *58*, 160-168.

Essafi-Benkhadir, K., Onesto, C., Stebe, E., Moroni, C., and Pages, G. (2007). Tristetraprolin inhibits Ras-dependent tumor vascularization by inducing vascular endothelial growth factor mRNA degradation. Molecular biology of the cell *18*, 4648-4658.

Garner, A.P., Weston, C.R., Todd, D.E., Balmanno, K., and Cook, S.J. (2002). Delta MEKK3:ER* activation induces a p38 alpha/beta 2-dependent cell cycle arrest at the G2 checkpoint. Oncogene *21*, 8089-8104.

Garon, E.B., Rizvi, N.A., Hui, R., Leighl, N., Balmanoukian, A.S., Eder, J.P., Patnaik, A., Aggarwal, C., Gubens, M., Horn, L.*, et al.* (2015). Pembrolizumab for the treatment of non-small-cell lung cancer. The New England journal of medicine *372*, 2018-2028.

Giannou, A.D., Marazioti, A., Kanellakis, N.I., Giopanou, I., Lilis, I., Zazara, D.E., Ntaliarda, G., Kati, D., Armenis, V., Giotopoulou, G.A.*, et al.* (2017). NRAS destines tumor cells to the lungs. EMBO Mol Med *9*, 672-686.

Gubin, M.M., Zhang, X., Schuster, H., Caron, E., Ward, J.P., Noguchi, T., Ivanova, Y., Hundal, J., Arthur, C.D., Krebber, W.J.*, et al.* (2014). Checkpoint blockade cancer immunotherapy targets tumour-specific mutant antigens. Nature *515*, 577-581.

Hall, M.P., Huang, S., and Black, D.L. (2004). Differentiation-induced colocalization of the KH-type splicing regulatory protein with polypyrimidine tract binding protein and the c-src pre-mRNA. Molecular biology of the cell *15*, 774-786.

Hardle, L., Bachmann, M., Bollmann, F., Pautz, A., Schmid, T., Eberhardt, W., Kleinert, H., Pfeilschifter, J., and Muhl, H. (2015). Tristetraprolin regulation of interleukin-22 production. Sci Rep *5*, 15112.

Herbst, R.S., Soria, J.C., Kowanetz, M., Fine, G.D., Hamid, O., Gordon, M.S., Sosman, J.A., McDermott, D.F., Powderly, J.D., Gettinger, S.N.*, et al.* (2014). Predictive correlates of response to the anti-PD-L1 antibody MPDL3280A in cancer patients. Nature *515*, 563-567.

Jiang, X.F., Zhou, J., Giobbie-Hurder, A., Wargo, J., and Hodi, F.S. (2013). The Activation of MAPK in Melanoma Cells Resistant to BRAF Inhibition Promotes PD-L1 Expression That Is Reversible by MEK and PI3K Inhibition. Clin Cancer Res *19*, 598-609.

Kataoka, K., Shiraishi, Y., Takeda, Y., Sakata, S., Matsumoto, M., Nagano, S., Maeda, T., Nagata, Y., Kitanaka, A., Mizuno, S.*, et al.* (2016). Aberrant PD-L1 expression through 3'-UTR disruption in multiple cancers. Nature *534*, 402-406.

Kemp, S.J., Thorley, A.J., Gorelik, J., Seckl, M.J., O'Hare, M.J., Arcaro, A., Korchev, Y., Goldstraw, P., and Tetley, T.D. (2008). Immortalization of Human Alveolar Epithelial Cells to Investigate Nanoparticle Uptake. Am J Resp Cell Mol *39*, 591-597.

Lai, W.S., Parker, J.S., Grissom, S.F., Stumpo, D.J., and Blackshear, P.J. (2006). Novel mRNA targets for tristetraprolin (TTP) identified by global analysis of stabilized transcripts in TTP-deficient fibroblasts. Molecular and cellular biology *26*, 9196-9208.

Lau, J., Cheung, J., Navarro, A., Lianoglou, S., Haley, B., Totpal, K., Sanders, L., Koeppen, H., Caplazi, P., McBride, J.*, et al.* (2017). Tumour and host cell PD-L1 is required to mediate suppression of anti-tumour immunity in mice. Nat Commun *8*, 14572.

Le, D.T., Uram, J.N., Wang, H., Bartlett, B.R., Kemberling, H., Eyring, A.D., Skora, A.D., Luber, B.S., Azad, N.S., Laheru, D.*, et al.* (2015). PD-1 Blockade in Tumors with Mismatch-Repair Deficiency. The New England journal of medicine *372*, 2509-2520.

Li, D., Zhu, X., Wang, H., and Li, N. (2017). Association between PD-L1 expression and driven gene status in NSCLC: A meta-analysis. Eur J Surg Oncol *43*, 1372-1379.

Linnemann, C., van Buuren, M.M., Bies, L., Verdegaal, E.M.E., Schotte, R., Calis, J.J.A., Behjati, S., Velds, A., Hilkmann, H., el Atmioui, D.*, et al.* (2015). High-throughput epitope discovery reveals frequent recognition of neo-antigens by CD4(+) T cells in human melanoma. Nat Med *21*, 81-85.

Lito, P., Solomon, M., Li, L.S., Hansen, R., and Rosen, N. (2016). Allele-specific inhibitors inactivate mutant KRAS G12C by a trapping mechanism. Science *351*, 604-608.

Liu, L., Mayes, P.A., Eastman, S., Shi, H., Yadavilli, S., Zhang, T.D., Yang, J.S., Seestaller-Wehr, L., Zhang, S.Y., Hopson, C.*, et al.* (2015). The BRAF and MEK Inhibitors Dabrafenib and Trametinib: Effects on Immune Function and in Combination with Immunomodulatory Antibodies Targeting PD-1, PD-L1, and CTLA-4. Clin Cancer Res *21*, 1639-1651.

Loboda, A., Nebozhyn, M., Klinghoffer, R., Frazier, J., Chastain, M., Arthur, W., Roberts, B., Zhang, T., Chenard, M., Haines, B.*, et al.* (2010). A gene expression signature of RAS pathway dependence predicts response to PI3K and RAS pathway inhibitors and expands the population of RAS pathway activated tumors. BMC Med Genomics *3*, 26.

Lykke-Andersen, J., and Wagner, E. (2005). Recruitment and activation of mRNA decay enzymes by two ARE-mediated decay activation domains in the proteins TTP and BRF-1. Genes & development *19*, 351-361.

Mahtani, K.R., Brook, M., Dean, J.L., Sully, G., Saklatvala, J., and Clark, A.R. (2001). Mitogen-activated protein kinase p38 controls the expression and posttranslational modification of tristetraprolin, a regulator of tumor necrosis factor alpha mRNA stability. Molecular and cellular biology *21*, 6461-6469.

Molina-Arcas, M., Hancock, D.C., Sheridan, C., Kumar, M.S., and Downward, J. (2013). Coordinate Direct Input of Both KRAS and IGF1 Receptor to Activation of PI3 Kinase in KRAS-Mutant Lung Cancer. Cancer discovery *3*, 548-563.

Nicke, B., Bastien, J., Khanna, S.J., Warne, P.H., Cowling, V., Cook, S.J., Peters, G., Delpuech, O., Schulze, A., Berns, K.*, et al.* (2005). Involvement of MINK, a Ste20 family kinase, in Ras oncogene-induced growth arrest in human ovarian surface epithelial cells. Mol Cell *20*, 673-685.

Pardoll, D.M. (2012). The blockade of immune checkpoints in cancer immunotherapy. Nat Rev Cancer *12*, 252-264.

Parsa, A.T., Waldron, J.S., Panner, A., Crane, C.A., Parney, I.F., Barry, J.J., Cachola, K.E., Murray, J.C., Tihan, T., Jensen, M.C.*, et al.* (2007). Loss of tumor suppressor PTEN function increases B7-H1 expression and immunoresistance in glioma. Nat Med *13*, 84-88.

Patricelli, M.P., Janes, M.R., Li, L.S., Hansen, R., Peters, U., Kessler, L.V., Chen, Y., Kucharski, J.M., Feng, J., Ely, T.*, et al.* (2016). Selective Inhibition of Oncogenic KRAS Output with Small Molecules Targeting the Inactive State. Cancer discovery *6*, 316-329.

Rajagopalan, L.E., Burkholder, J.K., Turner, J., Culp, J., Yang, N.S., and Malter, J.S. (1995). Granulocyte-macrophage colony-stimulating factor mRNA stabilization enhances transgenic expression in normal cells and tissues. Blood *86*, 2551-2558.

Rizvi, N.A., Hellmann, M.D., Snyder, A., Kvistborg, P., Makarov, V., Havel, J.J., Lee, W., Yuan, J.D., Wong, P., Ho, T.S.*, et al.* (2015). Mutational landscape determines sensitivity to PD-1 blockade in non-small cell lung cancer. Science *348*, 124-128.

Rounbehler, R.J., Fallahi, M., Yang, C., Steeves, M.A., Li, W., Doherty, J.R., Schaub, F.X., Sanduja, S., Dixon, D.A., Blackshear, P.J., and Cleveland, J.L. (2012). Tristetraprolin impairs myc-induced lymphoma and abolishes the malignant state. Cell *150*, 563-574.

Selamat, S.A., Chung, B.S., Girard, L., Zhang, W., Zhang, Y., Campan, M., Siegmund, K.D., Koss, M.N., Hagen, J.A., Lam, W.L.*, et al.* (2012). Genome-scale analysis of DNA methylation in lung adenocarcinoma and integration with mRNA expression. Genome research *22*, 1197-1211.

Skrzypczak, M., Goryca, K., Rubel, T., Paziewska, A., Mikula, M., Jarosz, D., Pachlewski, J., Oledzki, J., and Ostrowsk, J. (2010). Modeling Oncogenic Signaling in Colon Tumors by Multidirectional Analyses of Microarray Data Directed for Maximization of Analytical Reliability. Plos One *5*.

Stoecklin, G., Stubbs, T., Kedersha, N., Wax, S., Rigby, W.F., Blackwell, T.K., and Anderson, P. (2004). MK2-induced tristetraprolin:14-3-3 complexes prevent stress granule association and ARE-mRNA decay. EMBO J *23*, 1313-1324.

Stoecklin, G., Tenenbaum, S.A., Mayo, T., Chittur, S.V., George, A.D., Baroni, T.E., Blackshear, P.J., and Anderson, P. (2008). Genome-wide analysis identifies interleukin-10 mRNA as target of tristetraprolin. The Journal of biological chemistry *283*, 11689-11699.

Sumimoto, H., Takano, A., Teramoto, K., and Daigo, Y. (2016). RAS-Mitogen-Activated Protein Kinase Signal Is Required for Enhanced PD-L1 Expression in Human Lung Cancers. Plos One *11*.

Sun, L., Stoecklin, G., Van Way, S., Hinkovska-Galcheva, V., Guo, R.F., Anderson, P., and Shanley, T.P. (2007). Tristetraprolin (TTP)-14-3-3 complex formation protects TTP from dephosphorylation by protein phosphatase 2a and stabilizes tumor necrosis factor-alpha mRNA. The Journal of biological chemistry *282*, 3766-3777.

Sweet-Cordero, A., Mukherjee, S., Subramanian, A., You, H., Roix, J.J., Ladd-Acosta, C., Mesirov, J., Golub, T.R., and Jacks, T. (2005). An

oncogenic KRAS2 expression signature identified by cross-species gene-expression analysis. Nat Genet *37*, 48-55.

Taylor, G.A., Carballo, E., Lee, D.M., Lai, W.S., Thompson, M.J., Patel, D.D., Schenkman, D.I., Gilkeson, G.S., Broxmeyer, H.E., Haynes, B.F., and Blackshear, P.J. (1996). A pathogenetic role for TNF alpha In the syndrome of cachexia, arthritis, and autoimmunity resulting from tristetraprolin (TTP) deficiency. Immunity *4*, 445-454.

Taylor, G.A., Thompson, M.J., Lai, W.S., and Blackshear, P.J. (1995). Phosphorylation of tristetraprolin, a potential zinc finger transcription factor, by mitogen stimulation in intact cells and by mitogen-activated protein kinase in vitro. The Journal of biological chemistry *270*, 13341-13347.

Topalian, S.L., Hodi, F.S., Brahmer, J.R., Gettinger, S.N., Smith, D.C., McDermott, D.F., Powderly, J.D., Carvajal, R.D., Sosman, J.A., Atkins, M.B.*, et al.* (2012). Safety, activity, and immune correlates of anti-PD-1 antibody in cancer. The New England journal of medicine *366*, 2443-2454.

Yang, H., Chen, H., Luo, S., Li, L., Zhou, S., Shen, R., Lin, H., and Xie, X. (2017). The correlation between programmed death-ligand 1 expression and driver gene mutations in NSCLC. Oncotarget *8*, 23517-23528.

Yang, N.S., Wang, J.H., and Turner, J. (2004). Molecular strategies for improving cytokine transgene expression in normal and malignant tissues. Gene Ther *11*, 100-108.

Zubiaga, A.M., Belasco, J.G., and Greenberg, M.E. (1995). The nonamer UUAUUUAUU is the key AU-rich sequence motif that mediates mRNA degradation. Molecular and cellular biology *15*, 2219-2230.

Figure Legends

Figure 1. Cell-intrinsic Upregulation of PD-L1 through Oncogenic RAS Signalling

(**A**) Western blotting analysis of ER-KRAS^{G12V} type II pneumocytes treated with 4-OHT in starvation medium.

(**B**) qPCR analysis of ER-KRAS^{G12V} type II pneumocytes treated with 4-OHT or IFN-γ in starvation medium. Mean ± SEM of biological duplicates.

(**C**) Representative flow cytometry histogram of PD-L1 surface protein expression in ER-KRAS^{G12V} type II pneumocytes treated in starvation medium for 48 h.

(**D**) Western blotting analysis of RAS signalling following 5 h treatment with the KRAS^{G12C} inhibitor ARS853.

(**E**) qPCR analysis following 5 h treatment with the KRAS^{G12C} inhibitor ARS853 (10 μM). Mean ± SEM of biological duplicates.

(**F**) Flow cytometry analysis of PD-L1 surface protein expression in H358 cells treated with ARS853 (10 μM) for 48 h. Mean ± SEM of biological triplicates.

(**G**) Flow cytometry analysis of PD-L1 surface protein expression in ER-KRAS^{G12V} type II pneumocytes treated in starvation medium for 24 h. Mean ± SEM of two independent experiments.

(**H**) qPCR analysis from the experiment described in (G). Mean ± SEM of biological triplicates.

(**I**) qPCR analysis of H358 cells treated for 24 h. Mean ± SEM of two independent experiments.

(**J**) qPCR analysis of H358 cells treated with PMA for 3 h following a 30 min pre-treatment with DMSO or MEK inhibitor. Mean ± SD of two independent experiments.

MFI, Mean Fluorescence Intensity. EtOH, ethanol vehicle. 4-OHT, 100 nM. IFN-γ, 20 ng/ml. MEK inhibitor GSK1120212, 25 nM. PI3K inhibitor GDC-0941, 500 nM. PMA, 200 nM. ****P<0.0001, ***P<0.001, **P<0.01, *P<0.05, n.s; not significant. Unpaired, two-tailed Student's *t*-tests. See also Figure S1.

Figure 2. RAS Signalling Increases *PD-L1* mRNA Stability through AU-rich Elements in the 3'UTR

(**A**) qPCR analysis of *PD-L1* mRNA stability in ER-KRAS^{G12V} type II pneumocytes after the concomitant addition of actinomycin D (5 μg/ml or 10 μg/ml) and 4-OHT or vehicle added at time = 0 h in starvation medium. Mean ± SEM of two independent experiments. ***P<0.0005; Two-way ANOVA.

(**B**) qPCR analysis of *PD-L1* mRNA stability in KPB6 cells after the addition of actinomycin D (5 μg/ml) and DMSO or MEK inhibitor. Cells were pre-treated with DMSO or MEK inhibitor for 30 min before actinomycin D addition. Mean ± SEM of two independent experiments. ***P<0.0005; Two-way ANOVA.

(**C**) qPCR analysis of *PD-L1* mRNA stability after the addition of actinomycin D (5 μg/ml) and DMSO or ARS853. Cells were pre-treated with DMSO or ARS853 for 35 min before actinomycin D addition. Mean ± SEM of two independent experiments (n=2). ***P<0.0005; Two-way ANOVA.

(**D**) Sequence alignment of conserved AU-rich element ATTTA pentamer sequences (highlighted in red) in the mouse and human *PD-L1 3'UTR*.

(**E**) Normalised luciferase signal in ER-HRAS^{G12V} MCF10A cells from wild-type (ATTTA x 6) or mutant (ATGTA x 6) *PD-L1*-3'UTR reporters, 24 h after treatment in starvation medium. Mean ± SEM of three independent experiments.

(**F**) Normalised luciferase signal in H358 cells from wild-type (ATTTA x 6) or mutant (ATGTA x 6) *PD-L1*-3'UTR reporters, 6 h after treatment. Mean ± SEM of three independent experiments.

4-OHT, 100 nM. MEK inhibitor GSK1120212, 25 nM. PMA, 200 nM.

***P<0.0005, **P<0.005, *P<0.05, n.s; not significant. Unpaired, two-tailed Student's *t*-tests. See also Figure S2.

Figure 3. AU-rich element Binding Proteins TTP and KSRP are Negative Regulators of *PD-L1* Expression

(**A**-**C**) qPCR analysis 48 h after transfection with siRNAs targeting AU-rich element binding proteins (AU-BPs) relative to siScrambled (siSc) control. Mean ± SD of biological triplicates.

(**D**) qPCR and Western blotting analysis of H358 cells 24 h after transfection. qPCR data represent the mean ± SD of biological triplicates and are representative of two independent experiments. *, non-specific band.

(**E**) Normalised luciferase signal from the wild-type, *PD-L1*-3'UTR reporter 24 h after co-transfection with the indicated constructs. Mean ± SEM of two independent experiments.

(**F**) qPCR analysis of following serum stimulation in serum-starved TTP WT or TTP KO MEFs. Mean ± SEM of two independent experiments.

(**G**) qPCR analysis of *PD-L1* mRNA stability after the addition of actinomycin D (5 μg/ml) in TTP WT or TTP KO MEFs. Mean ± SEM of two independent experiments.

(**H**) Normalised luciferase signal in KPB6 TTP (tet-ON) cells wild-type (ATTTA x 6) or mutant (ATGTA x 6) *PD-L1*-3'UTR reporters, 7 h after treatment. Data represent the mean ± SEM of biological triplicates and are representative of two independent experiments.

MEK inhibitor, GSK1120212, 25 nM. Dox., doxycycline 1 μg/ml. ****P<0.0001, ***P<0.001, **P<0.01. Unpaired, two-tailed Student's t-tests. See also Figure S3.

Figure 4. RAS Regulates PD-L1 Expression through TTP

(**A**) qPCR analysis of H358 cells following siRNA-mediated knock-down of *TTP* (24 h) followed by MEK inhibition (24 h). Mean ± SEM of two independent experiments.

(**B**) qPCR analysis of ER-KRAS^{G12V} type II pneumocytes treated for 24 h in starvation medium. Mean ± SEM of three independent experiments.

(**C**) qPCR analysis of RNA-IP immunoprecipitates from H358 cells. Mean ± SEM from biological triplicates.

(**D**) Western blotting analysis of H358 cells expressing the indicated constructs. 6.5 h post-transfection, cells were treated with DMSO or MEK inhibitor for an additional 16 h. Arrow indicates Myc-TTP.

(**E**) Western blotting analysis of immunoprecipitations from H358 cells transfected with Myc-TTP. 6.5 h post-transfection, cells were treated with DMSO or MEK inhibitor for an additional 16 h. Arrow indicates Myc-TTP; * indicates co-precipitating protein.

(**F**) qPCR analysis of TTP WT or TTP KO MEFs treated with okadaic acid or DMSO for 2 h. Mean ± SEM of two independent experiments.

EtOH, ethanol vehicle. 4-OHT, 100 nM. Okadaic acid, OA, 1 μM. MEK inhibitor, GSK1120212, 25 nM. ****P<0.0001, ***P<0.001, **P<0.01. Unpaired, two-tailed Student's t-tests. See also Figure S4.

Figure 5. RAS-ROS-p38 Signalling Controls TTP Activity

(**A**) Histograms represent peak areas from extracted ion chromatograms for non-phosphorylated and phosphorylated peptides corresponding to S52 and S178 phosphosites of mouse TTP. Myc-TTP was immunoprecipitated from CT26 Myc-TTP (tet-ON) cells 1 h after the indicated treatment. Mean ± SD of technical triplicates. Representative of two independent biological experiments.

(**B**) qPCR analysis of ER-KRAS^{G12V} type II pneumocytes treated in starvation medium for 24 h. Mean ± SEM of four independent experiments.

(**C**) Representative flow cytometry histograms of PD-L1 surface protein expression in MCF10A ER-ΔMEKK3 cells treated in starvation medium for one day (1 d) or four days (4 d).

(**D**) Flow cytometry analysis of PD-L1 surface protein expression on ER-HRAS^{G12V} MCF10A cells (24 h) and ER-HRAS^{G12V} HKE-3 cells (48 h) after treatment in starvation medium.

(**E**) qPCR analysis of CT26 cells at 2 h or 24 h after MK2 inhibition with PF 3644022. Mean ± SEM of two independent experiments.

(**F**) Sequence alignments of the conserved phosphosites (highlighted red) targeted by MK2 in mouse (*Mm*) and human (*Hs*) TTP protein.

(**G**) Western blotting of immunoprecipitations from CT26 TTP KO cells harbouring tet-ON, WT or phospho-mutant, Myc-TTP constructs. Cells were treated with dox. for 24 h before the addition of PMA or DMSO for 1 h. Arrow indicates Myc-TTP.

(**H**) qPCR analysis of CT26 TTP KO cells harbouring tet-ON, WT or phospho-mutant, Myc-TTP constructs, treated with dox or vehicle for 48 h. Data represent the mean ± SEM of two independent experiments.

$^{**}P < 0.005$, $^{*}P < 0.05$. Unpaired, two-tailed Student's *t*-test. 4-OHT, 100 nM. NAC, N-acetyl-L-cysteine, 10 mM. PMA, 200 nM. MEK inhibitor, GSK1120212, 25 nM. MK2 inhibitor PF 3644022, 1 μM. MK2 inhibitor III ,1 μM. Dox., doxycycline, 1 μg/ml. See also Figure S5.

Figure 6. RAS Pathway Activation is Associated with PD-L1 Upregulation in Human Cancers

(**A**) Heat-maps showing fold change in expression of T cell function related genes between high and low RAS pathway activity cohorts of lung adenocarcinoma (LUAD) and colon adenocarcinoma (COAD) TCGA samples. *KRAS* mutation status (codons 12, 13 and 61) is indicated for each sample. Genes are ranked in order of significance. Wald test, DESeq2.

(**B**) Box-and-whisker plots comparing *PD-L1* expression in RAS high versus low pathway activity cohorts in LUAD and COAD using two independent RAS gene expression signatures. Wald test, DESeq2.

See also Figure S6.

Figure 7. Restoration of Tumour Cell TTP Expression Enhances Anti-tumour Immunity

(**A**) Western blotting analysis of CT26 Myc-TTP tet-ON cells expressing either empty vector or mouse *PD-L1* cDNA lacking the 3'UTR (PD-L1 Δ3'UTR), 24 h after treatment (Dox., 0.1 μg/ml or 1 μg/ml). Arrow indicates Myc-TTP.

(**B**) Representative flow cytometry histograms of PD-L1 surface protein expression in CT26 stable cells lines in (A), 72 h after treatment (Dox., 1 μg/ml). Data are representative of three independent experiments.

(**C**) Tumour growth curves for CT26-derived cell lines subcutaneously transplanted into BALB/c mice (n = 8 per group).

(**D**) Tumour growth curves for MC38-derived cell lines subcutaneously transplanted into C57BL/6 mice (n = 6 per group). X denotes the loss of a doxycycline-treated mouse.

(**E**) Tumour growth curves for CT26-derived cell lines subcutaneously transplanted into *nu/nu* mice (n = 6 per group).

(**F**) Tumour growth curves for CT26-derived cell lines subcutaneously transplanted into BALB/c mice (n = 4-5 per group).

For 7C-F, data represent the mean ± SEM. **P<0.01, ****P<0.0001, n.s., not significant; two-way ANOVA.

(**G**) Histological analysis of subcutaneous tumours at the end-point from the experiment described in (C), with quantification of CD3+ cells in 5 fields of view per mouse with 5-6 mice per group. Mean ± SEM. **P<0.01; unpaired, two-tailed Student's t-test.

(**H**) Quantification of $CD8^+$/Treg ratios and $CD8^+$ IFN-γ^+ cells from flow cytometry analysis of tumours after 18-20 days of growth. Each data point represents data from an individual mouse; mean ± SEM. **P*<0.05; unpaired, two-tailed Student's *t*-test.

(**I**) Proposed molecular model. Signalling nodes that influence anti-tumour immunity and are amenable to inhibition with drugs used in this study are highlighted. S52 and S178 represent MK2 target sites and numbering corresponds to mouse TTP. OA, Okadaic acid.

See also Figure S7.

STAR Methods

CONTACT FOR REAGENT AND RESOURCE SHARING

Further information and requests for resources and reagents should be directed to and will be fulfilled by the Lead Contact, Julian Downward (Julian.Downward@crick.ac.uk).

EXPERIMENTAL MODEL AND SUBJECT DETAILS

Cell Lines

Specific culture conditions and origin of all the cell lines used in this study are listed in the Key Resources Table and Table S2. Cell lines were authenticated by STR profiling by Cell Services at the Francis Crick Institute. Cells and antibodies used for *in vivo* studies were independently tested for common rodent pathogens and were certified pathogen-free.

In vivo studies

All studies were performed under a UK Home Office approved project license and in accordance with institutional welfare guidelines. For tumour studies, we used 8-10 week old BALB/c or *nu/nu* (*Foxn1*^{nu}) mice (for CT26 cells) or 16-17 week old C57BL/6 (for MC38 cells). Sex-matched mice were randomly assigned into experimental groups before tumour cell injection. Group sizes are indicated in the figure legends.

For autochthonous tumour formation, *Kras*$^{LSL\text{-}G12D/+}$; *Trp53*$^{F/F}$ mice were sourced from the Mouse Models of Human Cancer Consortium (B6.129-*Kras*^{tm4Tyj}/Nci and FVB.129P2-*Trp53*^{tm1Brn}/Nci) and were backcrossed to C57BL/6 for 6 generations. Lung tumours were initiated using intratracheal intubation of 1x10^6 pfu adenovirus expressing Cre-recombinase (Gene Transfer Vector Core) in mice between 6-12 weeks of age. Lung tumour or normal lung tissue was analysed 12 weeks after infection.

METHOD DETAILS

In vivo studies

Mice received 1x10^5 cells in PBS by subcutaneous injection into the left flank. Mice were treated with water or doxycycline by oral gavage (50 mg/kg) on day three after cell injection and then daily, with a two-day break every five days of treatment. For CD4$^+$ and CD8$^+$ cell depletion experiments, mice received 300 µg of GK1.5 and 300 µg of 2.43 monoclonal antibodies or rat IgG2b isotype control by i.p. administration three days before tumour cell engraftment and then twice weekly for the duration of the experiment. Depletion of CD8$^+$ and CD4$^+$ T cells was verified by flow cytometry using detection antibodies recognising distinct epitopes from the depletion antibodies. Tumours were measured using callipers and volume was estimated using the formula: width^2 x length x 0.5, where length is the longest dimension and width is the corresponding perpendicular dimension.

Transfections

For RNA interference, cells were reverse-transfected with a final concentration of 50 nM siGENOME siRNA pools or ON-TARGETplus Non-targeting pool ("SiScrambled" control) or 25 nM for single deconvoluted siRNAs, and DharmaFECT 1 transfection reagent (Dharmacon; GE Healthcare) in 96 well plates. For transfection with TTP or KSRP constructs, cells were seeded in a 12 well plate and the following day transfected using Lipofectamine 2000 (Life Technologies).

Cloning, plasmids and stable cell lines

peGFPC1-6XHis-FL-KSRP was a gift from Douglas Black (Addgene plasmid # 23001)(Hall et al., 2004) and the S193A mutant was generated by site-directed mutagenesis (QuikChange II; Agilent Technologies). Full length human TTP was cloned from H358 genomic DNA into pcDNA3-MycX2 generating two N-terminal Myc tags. The S218 S228A TTP human and S52A S178A mouse double mutant constructs were generated by site-directed mutagenesis (QuikChange II; Agilent Technologies).

For the human PD-L1 (*CD274* gene) we refer to GRCh38:CM000671.2. For human *PD-L1* mRNA we refer to NM_014143. For mouse PD-L1 (*Cd274* gene) we refer to GRCm38:CM001012.2. For mouse *PD-L1* mRNA we refer to NM_021893. For the 3'UTR luciferase reporter constructs, the full length human *PD-L1* 3'UTR was cloned from H358 genomic DNA into the TOPO-TA vector (Life Technologies). The six most 3' ATTTA pentamers (including the three most highly conserved, as shown in

Figure 2D) were mutated to ATGTA (QuikChange Multi-site; Agilent). Wild type and mutant fragments were subcloned into the Xba1, BamH1 site of pGL3-Control (Promega) to generate the reporter constructs.

CT26 cells were transfected with linearised pUNO empty and pUNO-mouse *PD-L1*Δ3'UTR plasmids (InvivoGen) before selection with blasticidin, and for *PD-L1*Δ3'UTR cells, subsequent FACS sorting of PD-L1 high, blasticidin-resistant cells. PD-L1 + wild type 3'UTR was subcloned from pCDNA3.1 mouse ORF clone NM_021893.3 (Creative Biogene) into the pUNO vector, linearised and transfected into CT26 cells to generate a stable cell line following selection with blasticidin and sorting for PD-L1 high cells.
For the lentiviral pTRIPZ constructs, full-length mouse TTP was cloned from KPB6 genomic DNA into pcDNA3-MycX2 generating two N-terminal Myc tags. MycX2-TTP was subsequently subcloned into the Age1-Mlu1 site of pTRIPZ-empty (GE Healthcare), resulting in the final TTP (tet-ON) construct, without the TurboRFP or shRNAmir-related elements of the parental pTRIPZ plasmid. Lentiviral particles were produced by co-transfection of 293FT cells with pTRIPZ-TTP, psPAX2 and pMD2.G plasmids and the infected CT26 or MC38 target cells were selected with puromycin to establish stable cell lines.
For CD274 promoter reporter constructs, pGL3-Basic (Promega) served as a negative control and pGL3-Control (Promega) served as a positive control for firefly luciferase expression. The indicated fragments of the human CD274 promoter region were cloned from H358 genomic DNA into the MluI – XhoI site of pGL3-Basic. In addition, the putative enhancer site in intron 1 of the human CD274 gene was cloned into the BamH1 – SalI site (downstream of

the firefly luciferase ORF) of the 1 kb CD274 promoter pGL3-Basic reporter construct, as shown in Figure S2A. Sequencing of these constructs and comparison to the GRCh38 assembly revealed two documented SNPs in the putative enhancer region fragment: rs4742097 and rs2282055.

Flow cytometry

Lung tissue was harvested in ice-cold PBS before mincing and then enzymatic digestion in Liberase TM and Liberase TH (both 75 *μ*g/ml final; Roche) or collagenase I (1 mg/ml) with DNaseI (25 *μ*g/ml final; Sigma) in HBSS (Gibco) for 45 min at 37 ºC. After washing in DMEM + 10 % FCS, cells were filtered through 70 *μ*m filters (BD Bioscience) and then washed in FACS buffer (PBS supplemented with 2 mM EDTA and 0.5 % BSA v/v final). Samples were then treated with Red Blood Cell Lysis Buffer (Qiagen), washed in FACS buffer, filtered again and resuspended with FcR blocking reagent (BD Bioscience) before antibody staining of cell surface antigens in FACS buffer. For unfixed cells, samples were washed twice in FACS buffer and resuspended in DAPI (1 *μ*g/ml final; eBioscience) immediately before analysis on LSRII or LSRFortessa (BD Biosciences) cell analysers. Intracellular staining for Foxp3 and IFN-γ was performed on fixed cells using the Foxp3 Staining Set (eBiosicence) according to manufacturer's instructions. $CD4^+$ Tregs were defined by Foxp3 positivity. For IFN-γ staining, cells were stimulated for 4 h *ex-vivo* with PMA (20 ng/ml) and ionomycin (1 μg/ml) in the presence of GolgiPlug (BD Biosciences). Dead cells were excluded using the fixable viability dye eFluor 780 (eBioscience).

For FACS analysis of cells lines, cells were harvested with trypsin, washed in media and filtered before antibody staining in FACS buffer. Samples were washed twice in FACS buffer and resuspended in DAPI (1 μg/ml final; eBioscience) immediately before analysis. For the detection of intracellular ROS, adherent cells were washed in PBS before staining in 5 μM H_2DCFDA for 20 min in PBS at 37 °C. Cells were then harvested by trypsinisation and prepared for flow cytometry as described above.

Immunoprecipitation

For each immunoprecipitation reaction, 25 μl slurry of Dynabeads (Life Technologies) were coupled with 3 μg of anti-Myc antibody (9E10; in-house) or normal mouse IgG. For Figure 5H, cross-linking was performed using DSS following manufacturer's instructions (ThermoFisher). Beads were washed in Lysis Buffer (20 mM Tris-HCl, pH 7.4, 137.5 mM NaCl, 10 % glycerol, 1 % Triton X-100) and incubated overnight with rotation at 4 ºC with cleared cell lysates prepared in Lysis Buffer supplemented with protease and phosphatase inhibitor cocktails (Calbiochem). Beads were washed three times with IP Wash Buffer (modified Lysis Buffer: 0.1 % Triton X-100, final), before elution with LDS Sample Buffer (Life Technologies).

Immunohistochemistry

Tissue was prepared for histology by incubation in 10 % NBF for 24 h followed by 70 % ethanol for a further 24 h before embedding in paraffin. For CD3 staining, sections were boiled in sodium citrate buffer (pH6) for 15 min

and incubated for 1 h in anti-CD3 antibody (ab134096; Abcam), followed by biotinylated secondary antibody and HRP/DAB detection. Tumours from *nu/nu* mice served as a negative control for CD3 staining. Hematoxylin and eosin staining was performed using standard methods.

CRISPR/Cas

The CRISPR/Cas genome editing was performed on CT26 cells using a U6gRNA-Cas9-2A-GFP construct targeting mouse *Zfp36* with a gRNA sequence GTCATGGCTCATCGACTGGAGG (Sigma, MM0000323992). Following plasmid transfection, single GFP-positive cells were selected by FACS for expansion in culture. Transfection with Cas9-2A-GFP only served as a negative control. KO of functional TTP was confirmed by Western blotting and complete *Zfp36* allele disruption was confirmed by TOPO-TA cloning followed by sequencing.

Bioinformatics

Using two published RAS activation gene expression signatures (Loboda et al., 2010; Sweet-Cordero et al., 2005), we identified high and low RAS pathway activity LUAD TCGA RNASeq samples. We determined high and low RAS pathway activity using GSEA (GeneSetTest, Bioconductor) against genes ranked by their log2 normalized counts scaled across all tumour samples. Only the upregulated genes from the signatures were used in the GSEA. Samples with a significant GSEA association (FDR < 0.05) of a RAS signature to the upper portion of the rank were assigned as having high

RAS activity. Those with a significant association to the lower portion of the rank were assigned as having low RAS activity. Once assigned, we identified RAS-dependent gene expression changes between the high and low RAS activity groups by standard RNASeq analysis methods (DESeq2, FDR < 0.05). A short-list of “T cell Function” related genes was generated from gene ontology annotation based on the nanoString Technologies nCounter Human PanCancer Immune Profiling Panel.

Mass Spectrometry

Gel bands were excised and subjected to digestion with trypsin. Tryptic peptides were analysed by LC-MS using Ultimate 3000 uHPLC system connected to a Q-Exactive mass spectrometer (Thermo Fisher Scientific) and acquired in data-dependent mode (DDA) for identification and in targeted SIM/PRM mode for quantification. A SIM isolation list was setup for the following peptides: STSLVEGR (m/z 424.7272, 2+, non phos), STSLVEGR (m/z 464.7104, 2+, phos S52), QSISFSGLPSGR (m/z 618.3276, 2+, non phos) and QSISFSGLPSGR (m/z 658.3057, 2+, phos S178). For SIM/PRM scans, MS1 peaks were acquired at resolution of 70,000 (at m/z 200) and scan time (1x256 ms); MS2 fragment ion resolution was 17,500 (at m/z 200) scan time (64x4 ms); and SIM/PRM cycle time was (1280 ms). For identification and generation of spectral libraries, the resulting DDA data was searched against a mouse Uniprot database containing common contaminants (UniProt_KB2012_08_taxonomy_mouse_10090_canonical_with_contaminant

s.fasta) as well as a custom database containing the Myc-tagged mouse Zfp36 sequence using the Andromeda search engine and MaxQuant (version 1.3.0.5). For MaxQuant, a false discovery rate of 0.1 % was used to generate protein, peptide and site identification tables. The targeted mass spectrometry raw data was uploaded into Skyline (version 3.5.0.9319) for identification, quantification and further statistical analyses.

Western blotting

Western blotting was performed using standard methods. Primary antibodies used are listed in the Key Resources Table. Secondary antibodies were conjugated to horseradish peroxidase (GE Healthcare).

Luciferase assays

H358, ER-HRAS^{G12V} MCF10A and KP (tetON) cells were plated in 96 well plates and the following day co-transfected with pRL-TK control and pGL3-*3'UTR PD-L1* luciferase constructs using Lipofectamine 2000 (Life Technologies). 24 h after transfection, PMA (200 nM; Sigma), doxycycline (1 *μ*g/ml; Sigma) or MEK inhibitor GSK1120212 (25 nM; Selleckchem) was added, and 6-7 h later the Dual-Luciferase Reporter Assay (Promega) was performed. For ER-HRAS^{G12V} MCF10A, 24 h after transfection cells were serum-starved overnight, and then treated with 4-OHT (100 nM) for 24 h before the Dual-Luciferase Reporter Assay (Promega) was performed.

Quantitative real-time PCR (qPCR)

RNA was extracted using RNeasy Mini Kit (QIAGEN), cDNA was generated using SuperScript VILO or SuperScript II Reverse Transcriptase (Life Technologies) and qPCR reactions were carried out using QuantiTect Primer Assays (QIAGEN) and SYBR Green reagents (Life Technologies). Gene expression changes relative to the stated housekeeping gene were calculated using the ΔΔCT method.

RNA-immunoprecipitation

RNA-immunoprecipitation (RNA-IP) reactions were carried out using Magna-RIP RNA-IP Kit (Millipore) with IgG control, anti-TTP or anti-KSRP antibodies according to the manufacturer's instructions, except for the exclusion of EDTA from lysis and wash buffers, as TTP is a zinc-finger protein. Total RNA was isolated and qPCR was carried out using methods specified in the above section, except using the % input method to calculate RNA enrichment.

QUANTIFICATION AND STATISTICAL ANALYSIS

Statistical tests, *p*-values, replicates and the definition of centre and dispersion are indicated in the figures and figure legends. Unless otherwise stated in the figure legend, we used an unpaired, two-tailed Student's *t*-test, where statistical significance was defined by $P<0.05$. Statistical analyses were carried out in GraphPad Prism 7.

Figure 1

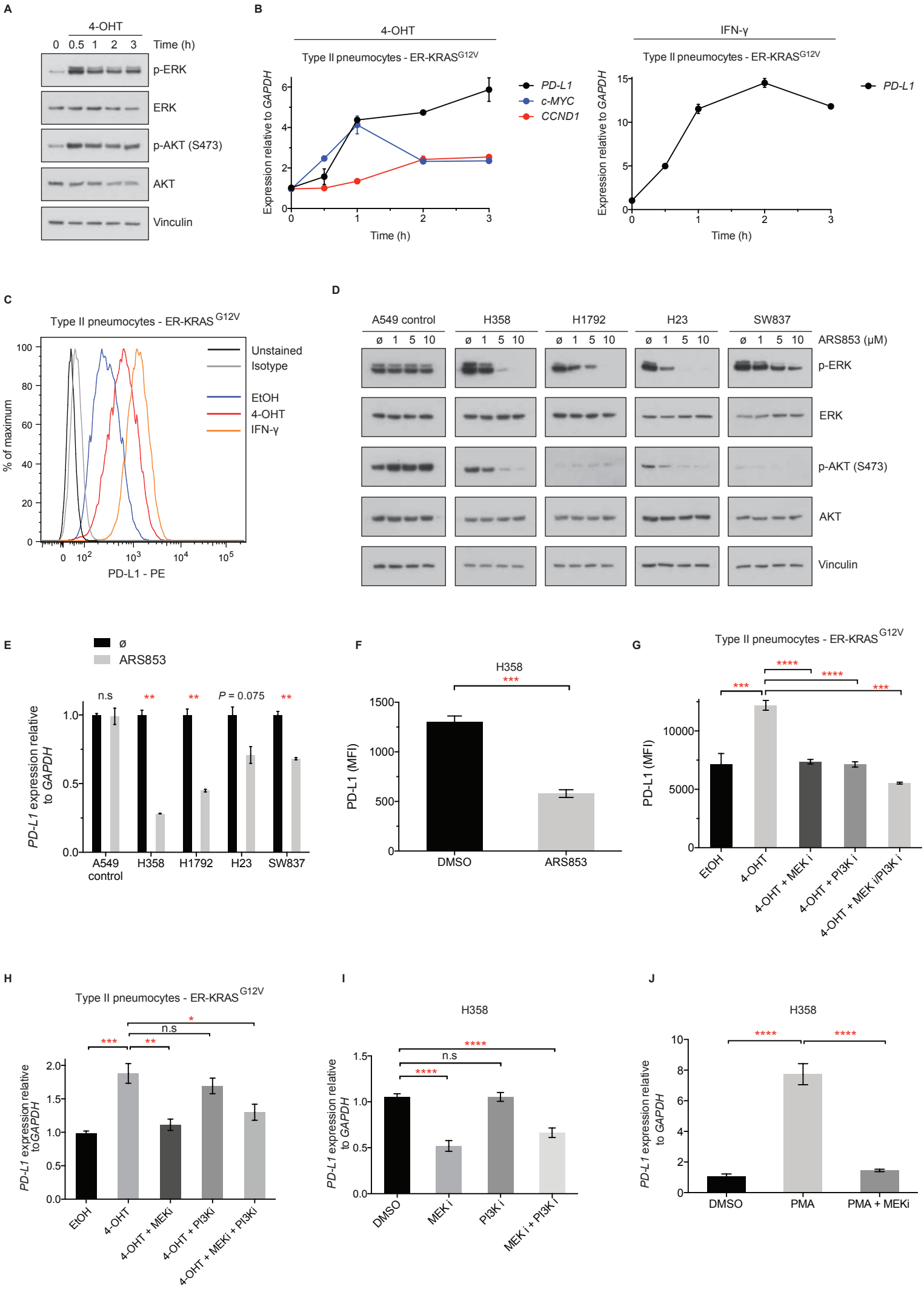
A
4-OHT
0 0.5 1 2 3 Time (h)
p-ERK
ERK
p-AKT (S473)
AKT
Vinculin
B
4-OHT
Type II pneumocytes - ER-KRAS G12V
Expression relative to GAPDH
PD-L1
c-MYC
CCND1
Time (h)
IFN-γ
Type II pneumocytes - ER-KRAS G12V
Expression relative to GAPDH
PD-L1
Time (h)
C
Type II pneumocytes - ER-KRAS G12V
% of maximum
Unstained
Isotype
EtOH
4-OHT
IFN-γ
PD-L1 - PE
D
A549 control
H358
H1792
H23
SW837
ø 1 5 10
ARS853 (μM)
p-ERK
ERK
p-AKT (S473)
AKT
Vinculin
E
ø
ARS853
n.s
**
**
P = 0.075
**
PD-L1 expression relative to GAPDH
A549 control
H358
H1792
H23
SW837
F
H358
***
PD-L1 (MFI)
DMSO
ARS853
G
Type II pneumocytes - ER-KRAS G12V
***
****
****
***
PD-L1 (MFI)
EtOH
4-OHT
4-OHT + MEK i
4-OHT + PI3K i
4-OHT + MEK i/PI3K i
H
Type II pneumocytes - ER-KRAS G12V
*
n.s
***
**
PD-L1 expression relative to GAPDH
EtOH
4-OHT
4-OHT + MEKi
4-OHT + PI3Ki
4-OHT + MEKi + PI3Ki
I
H358
****
n.s
****
PD-L1 expression relative to GAPDH
DMSO
MEK i
PI3K i
MEK i + PI3K i
J
H358
****
****
PD-L1 expression relative to GAPDH
DMSO
PMA
PMA + MEKi

Figure 2

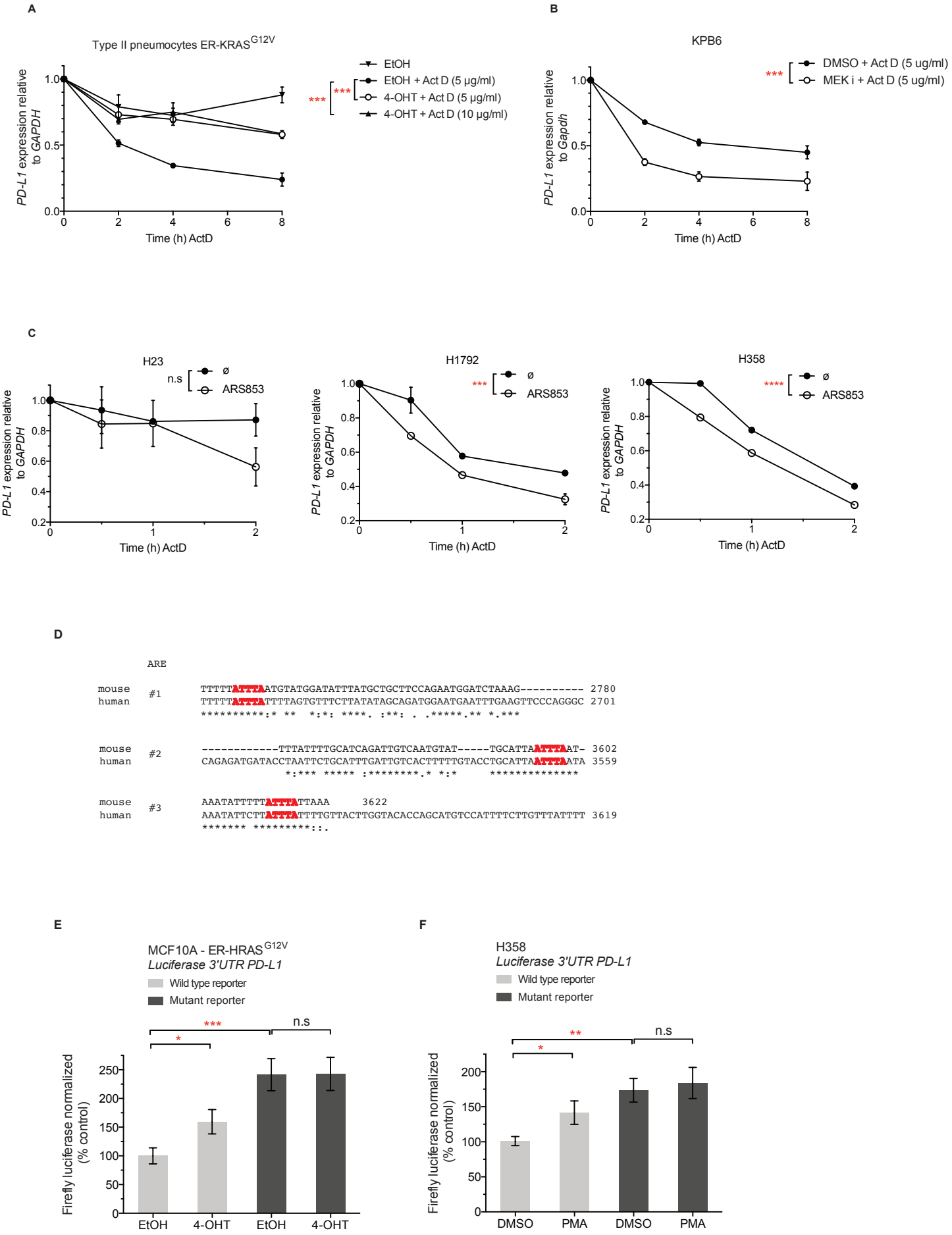
A
Type II pneumocytes ER-KRAS^{G12V}
PD-L1 expression relative to GAPDH
Time (h) ActD
EtOH
EtOH + Act D (5 µg/ml)
4-OHT + Act D (5 µg/ml)
4-OHT + Act D (10 µg/ml)
***
***
B
KPB6
PD-L1 expression relative to Gapdh
Time (h) ActD
DMSO + Act D (5 ug/ml)
MEK i + Act D (5 ug/ml)
***
C
H23
n.s
ø
ARS853
H1792
***
H358
****
PD-L1 expression relative to GAPDH
Time (h) ActD
D
ARE
mouse #1 TTTTTATTTAATGTATGGATATTTATGCTGCTTCCAGAATGGATCTAAAG---------- 2780
human #1 TTTTTATTTATTTTAGTGTTTCTTATATAGCAGATGGAATGAATTTGAAGTTCCCAGGGC 2701
mouse #2 ----------TTTATTTTGCATCAGATTGTCAATGTAT-----TGCATTAATTTAAT- 3602
human #2 CAGAGATGATACCTAATTCTGCATTTGATTGTCACTTTTTGTACCTGCATTAATTTAATA 3559
mouse #3 AAATATTTTTATTTATTAAA 3622
human #3 AAATATTCTTATTTATTTTGTTACTTGGTACACCAGCATGTCCATTTTCTTGTTTATTTT 3619
E
MCF10A - ER-HRAS^{G12V}
Luciferase 3'UTR PD-L1
Wild type reporter
Mutant reporter
Firefly luciferase normalized (% control)
EtOH
4-OHT
EtOH
4-OHT
F
H358
Luciferase 3'UTR PD-L1
DMSO
PMA
DMSO
PMA

Figure 3

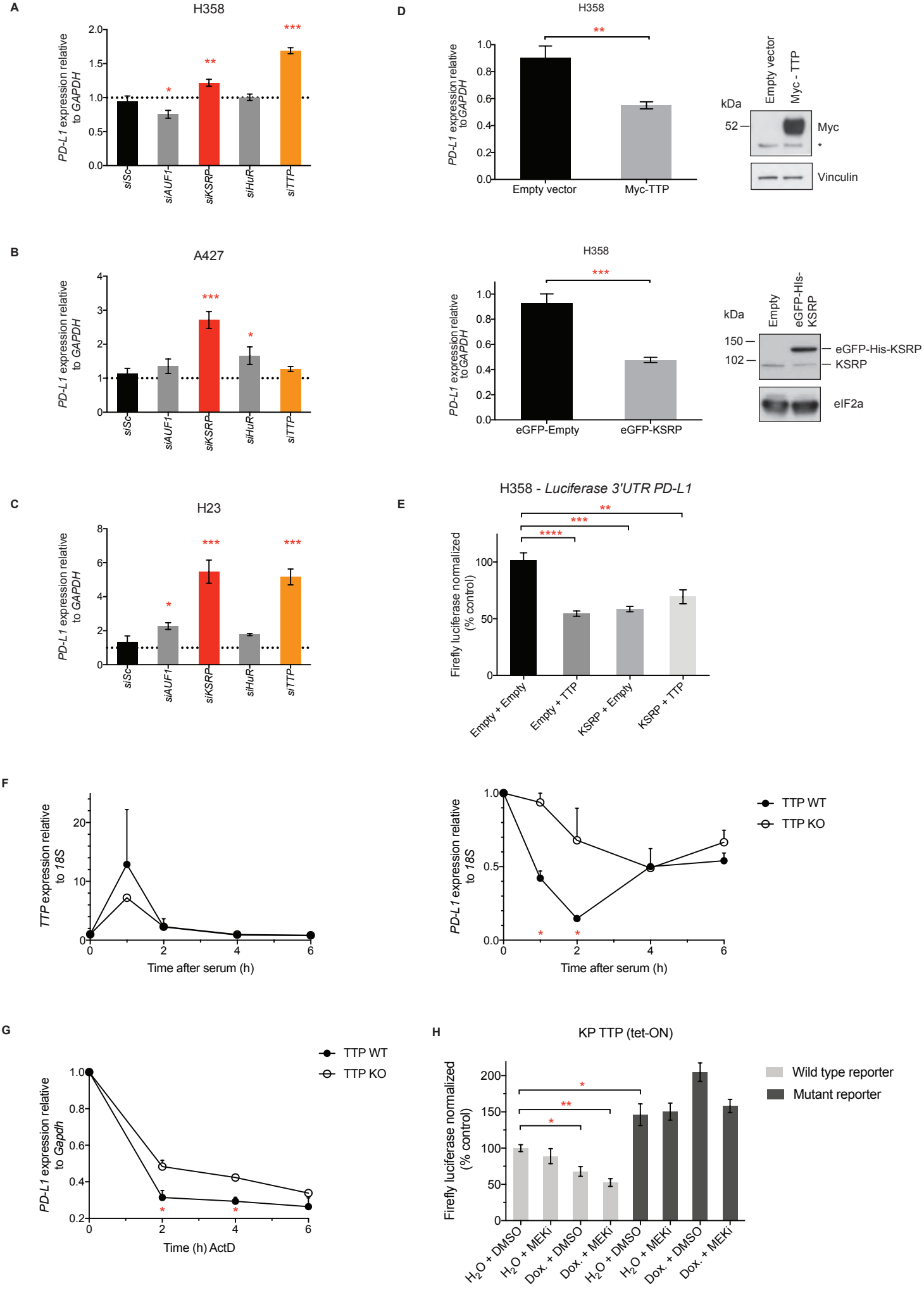
A
H358
PD-L1 expression relative to GAPDH
siSc
siAUF1
siKSRP
siHuR
siTTP
B
A427
C
H23
D
H358
Empty vector
Myc-TTP
kDa
52
Myc
Vinculin
H358
eGFP-Empty
eGFP-KSRP
150
102
eGFP-His-KSRP
KSRP
eIF2a
E
H358 - Luciferase 3'UTR PD-L1
Firefly luciferase normalized (% control)
Empty + Empty
Empty + TTP
KSRP + Empty
KSRP + TTP
F
TTP expression relative to 18S
Time after serum (h)
PD-L1 expression relative to 18S
TTP WT
TTP KO
G
PD-L1 expression relative to Gapdh
Time (h) ActD
H
KP TTP (tet-ON)
H2O + DMSO
H2O + MEKi
Dox. + DMSO
Dox. + MEKi
Wild type reporter
Mutant reporter

Figure 4

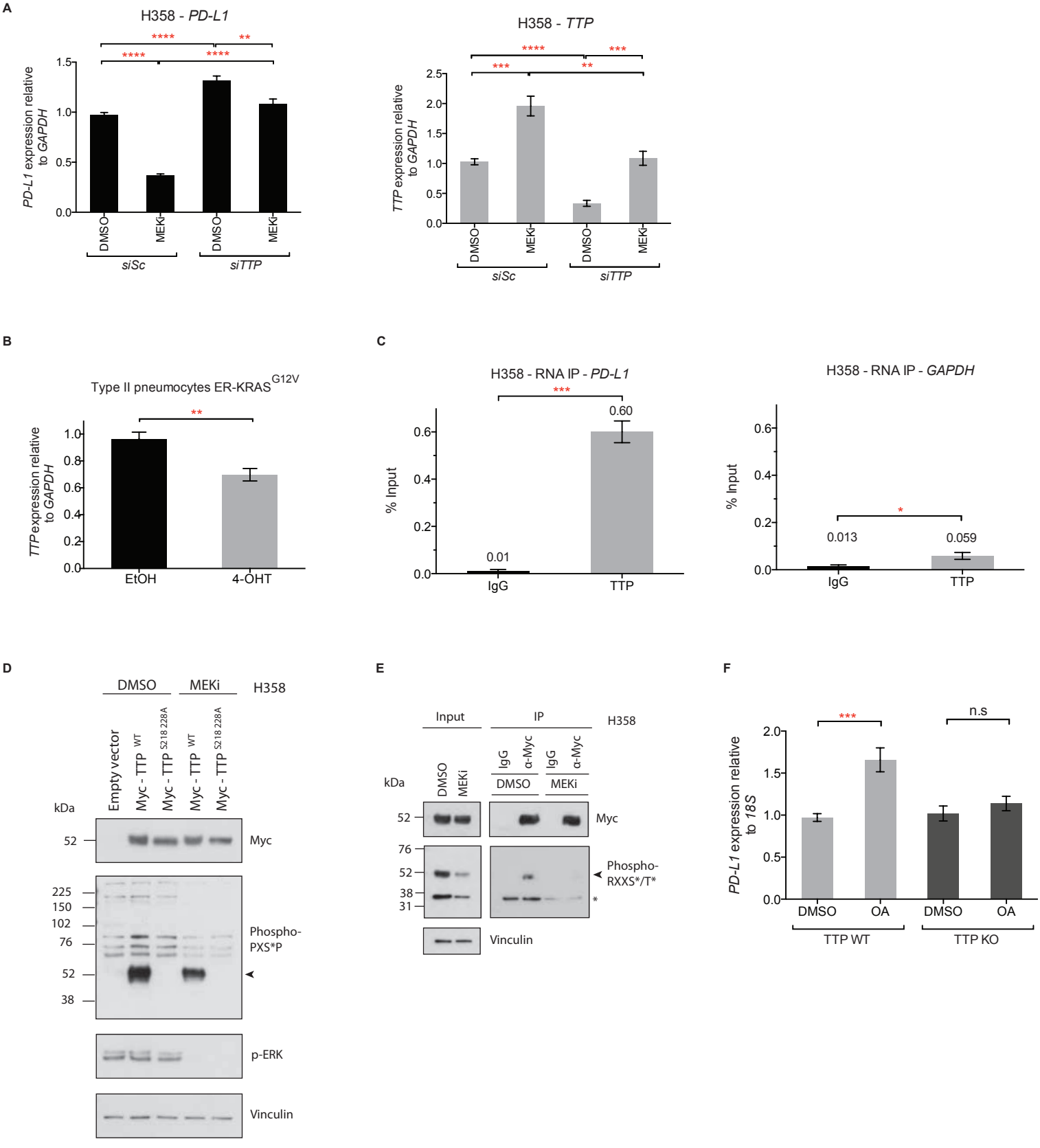
A
H358 - PD-L1
PD-L1 expression relative to GAPDH
DMSO
MEKi
siSc
siTTP
H358 - TTP
TTP expression relative to GAPDH
B
Type II pneumocytes ER-KRASG12V
TTP expression relative to GAPDH
EtOH
4-OHT
C
H358 - RNA IP - PD-L1
% Input
IgG
TTP
H358 - RNA IP - GAPDH
D
H358
Empty vector
Myc - TTP WT
Myc - TTP S218 228A
kDa
Myc
Phospho-PXS*P
p-ERK
Vinculin
E
Input
IP
H358
IgG
α-Myc
Phospho-RXXS*/T*
F
PD-L1 expression relative to 18S
n.s
OA
TTP WT
TTP KO

Figure 5

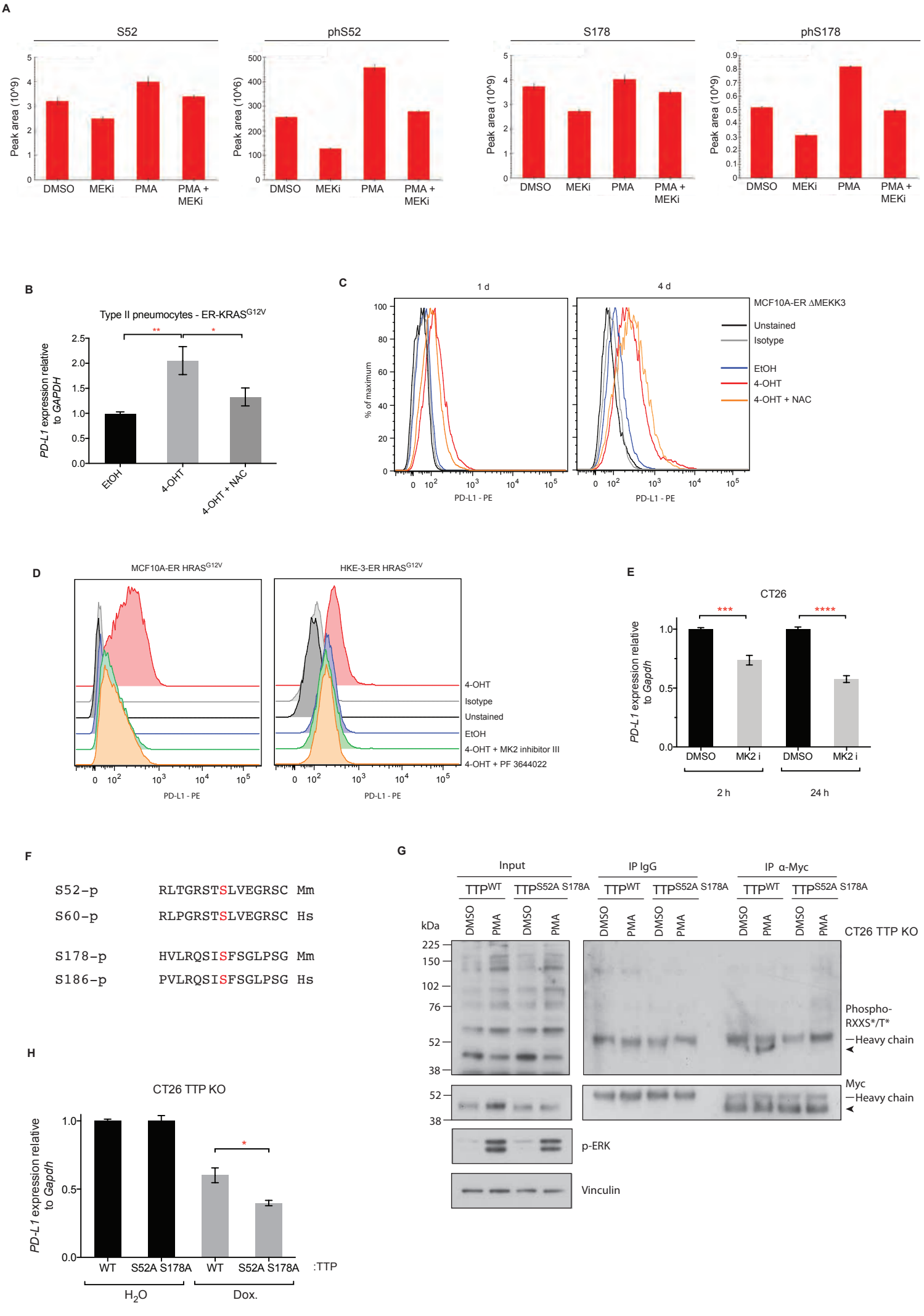
A
S52
phS52
S178
phS178
Peak area (10^9)
Peak area (10^6)
DMSO
MEKi
PMA
PMA + MEKi
B
Type II pneumocytes - ER-KRASG12V
PD-L1 expression relative to GAPDH
EtOH
4-OHT
4-OHT + NAC
C
1 d
4 d
% of maximum
PD-L1 - PE
MCF10A-ER ΔMEKK3
Unstained
Isotype
EtOH
4-OHT
4-OHT + NAC
D
MCF10A-ER HRASG12V
HKE-3-ER HRASG12V
4-OHT
Isotype
Unstained
EtOH
4-OHT + MK2 inhibitor III
4-OHT + PF 3644022
E
CT26
PD-L1 expression relative to Gapdh
DMSO
MK2 i
2 h
24 h
F
S52-p RLTGRSTSLVEGRSC Mm
S60-p RLPGRSTSLVEGRSC Hs
S178-p HVLRQSISFSGLPSG Mm
S186-p PVLRQSISFSGLPSG Hs
G
Input
IP IgG
IP α-Myc
TTPWT
TTPS52A S178A
kDa
CT26 TTP KO
Phospho-RXXS*/T*
Heavy chain
Myc
p-ERK
Vinculin
H
CT26 TTP KO
PD-L1 expression relative to Gapdh
WT
S52A S178A
:TTP
H2O
Dox.

Figure 6

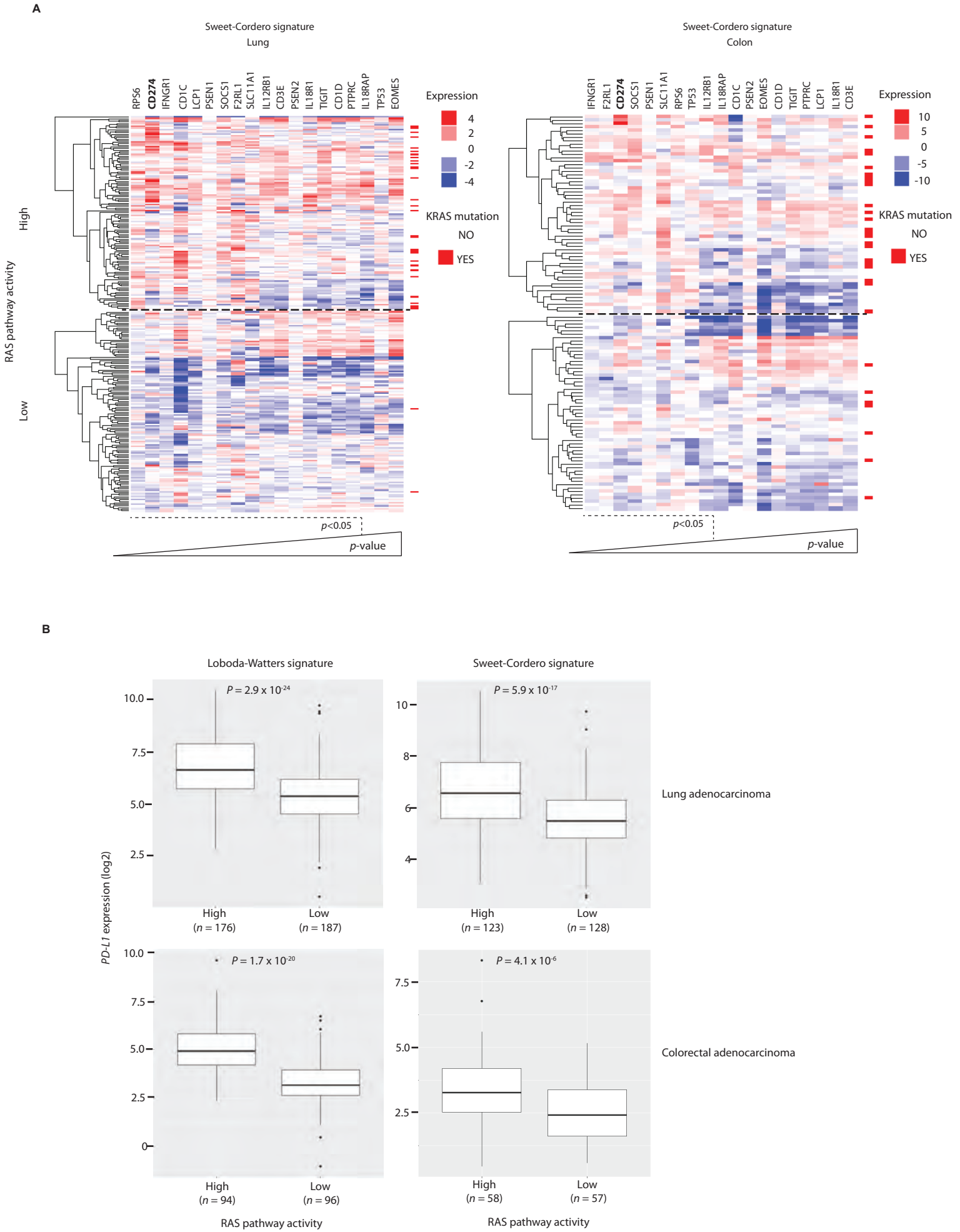
A
Sweet-Cordero signature
Lung
RPS6
CD274
IFNGR1
CD1C
LCP1
PSEN1
SOCS1
F2RL1
SLC11A1
IL12RB1
CD3E
PSEN2
IL18R1
TIGIT
CD1D
PTPRC
IL18RAP
TP53
EOMES
Expression
4
2
0
-2
-4
KRAS mutation
NO
YES
RAS pathway activity
High
Low
p<0.05
p-value
Sweet-Cordero signature
Colon
IFNGR1
F2RL1
CD274
SOCS1
PSEN1
SLC11A1
RPS6
TP53
IL12RB1
IL18RAP
CD1C
PSEN2
EOMES
CD1D
TIGIT
PTPRC
LCP1
IL18R1
CD3E
Expression
10
5
0
-5
-10
KRAS mutation
NO
YES
p<0.05
p-value
B
Loboda-Watters signature
Sweet-Cordero signature
P = 2.9 x 10-24
P = 5.9 x 10-17
PD-L1 expression (log2)
10.0
7.5
5.0
2.5
10
8
6
4
High
(n = 176)
Low
(n = 187)
High
(n = 123)
Low
(n = 128)
Lung adenocarcinoma
P = 1.7 x 10-20
P = 4.1 x 10-6
10.0
7.5
5.0
2.5
0
7.5
5.0
2.5
High
(n = 94)
Low
(n = 96)
High
(n = 58)
Low
(n = 57)
Colorectal adenocarcinoma
RAS pathway activity
RAS pathway activity

Figure 7

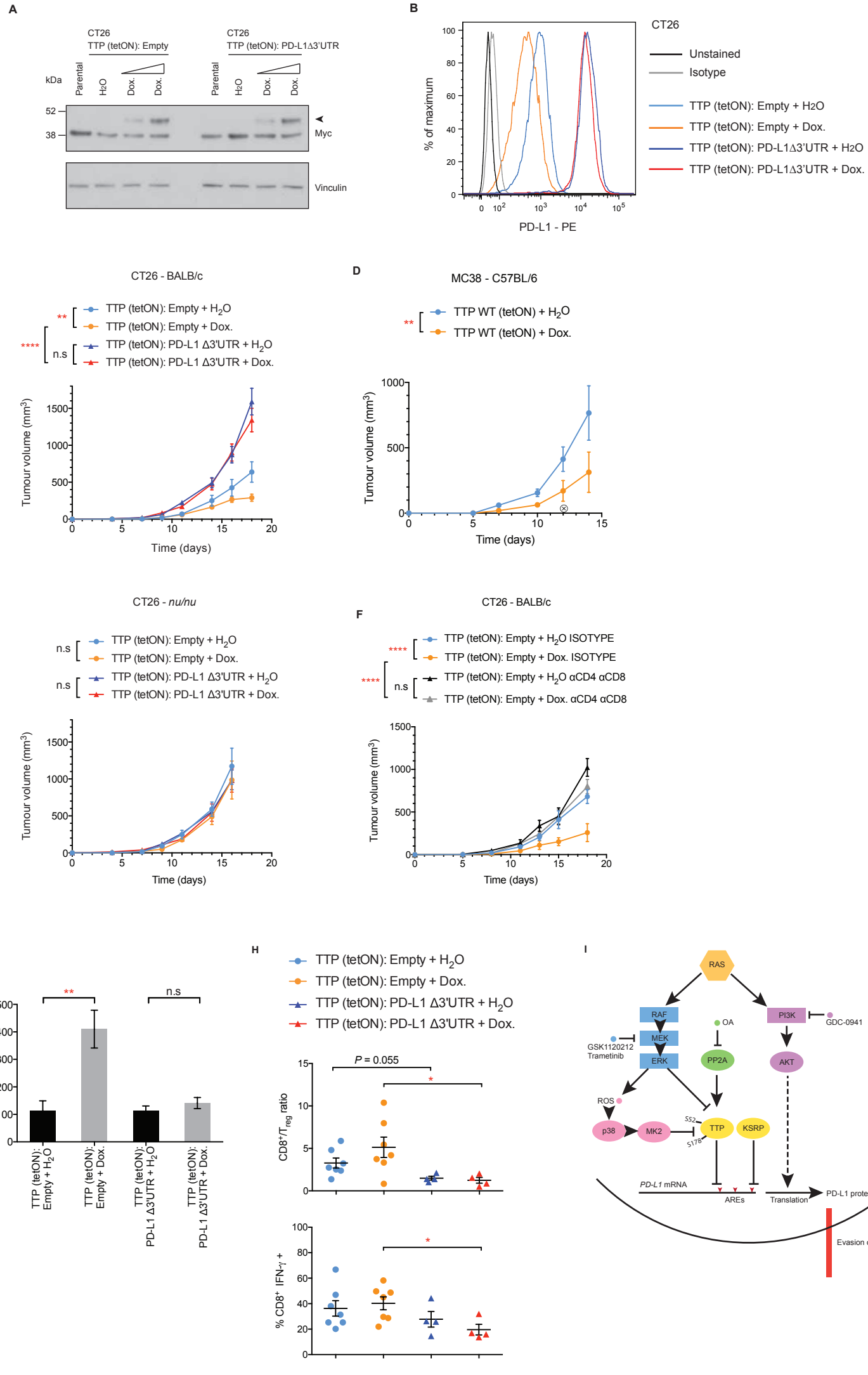
A
CT26
TTP (tetON): Empty
CT26
TTP (tetON): PD-L1Δ3'UTR
kDa
Parental
H2O
Dox.
Dox.
52
38
Myc
Vinculin
B
CT26
Unstained
Isotype
TTP (tetON): Empty + H2O
TTP (tetON): Empty + Dox.
TTP (tetON): PD-L1Δ3'UTR + H2O
TTP (tetON): PD-L1Δ3'UTR + Dox.
% of maximum
PD-L1 - PE
C
CT26 - BALB/c
**
****
n.s
TTP (tetON): Empty + H2O
TTP (tetON): Empty + Dox.
TTP (tetON): PD-L1 Δ3'UTR + H2O
TTP (tetON): PD-L1 Δ3'UTR + Dox.
Tumour volume (mm3)
Time (days)
D
MC38 - C57BL/6
**
TTP WT (tetON) + H2O
TTP WT (tetON) + Dox.
Tumour volume (mm3)
Time (days)
E
CT26 - nu/nu
n.s
n.s
TTP (tetON): Empty + H2O
TTP (tetON): Empty + Dox.
TTP (tetON): PD-L1 Δ3'UTR + H2O
TTP (tetON): PD-L1 Δ3'UTR + Dox.
Tumour volume (mm3)
Time (days)
F
CT26 - BALB/c
****
****
n.s
TTP (tetON): Empty + H2O ISOTYPE
TTP (tetON): Empty + Dox. ISOTYPE
TTP (tetON): Empty + H2O αCD4 αCD8
TTP (tetON): Empty + Dox. αCD4 αCD8
Tumour volume (mm3)
Time (days)
G
**
n.s
CD3+ cells/mm2 tumour
TTP (tetON): Empty + H2O
TTP (tetON): Empty + Dox.
TTP (tetON): PD-L1 Δ3'UTR + H2O
TTP (tetON): PD-L1 Δ3'UTR + Dox.
H
TTP (tetON): Empty + H2O
TTP (tetON): Empty + Dox.
TTP (tetON): PD-L1 Δ3'UTR + H2O
TTP (tetON): PD-L1 Δ3'UTR + Dox.
P = 0.055
*
CD8+/Treg ratio
*
% CD8+ IFN-γ +
I
RAS
RAF
MEK
ERK
PI3K
GDC-0941
OA
GSK1120212
Trametinib
PP2A
AKT
ROS
p38
MK2
S52
S178
TTP
KSRP
PD-L1 mRNA
AREs
Translation
PD-L1 protein
TUMOUR CELL
Evasion of the immune system

Supplemental Figure Legends

Figure S1, related to Figure 1. Cell-intrinsic Upregulation of PD-L1 through Oncogenic RAS Signalling

(**A**) qPCR analysis of *PD-L1* mRNA expression at 6 h and 24 h after addition of 4-OHT or EtOH vehicle in ER-HRAS^{G12V} MCF10A cells. Mean ± SEM of two independent experiments. ****P<0.0001; unpaired, two-tailed Student's *t*-tests.

(**B**) Flow cytometry analysis of PD-L1 surface protein expression at 24 h and four days after addition of 4-OHT or EtOH vehicle in ER-HRAS^{G12V} MCF10A cells and four days in ER-HRAS^{G12V} HKE-3 cells.

(**C**) Flow cytometry analysis of PD-L1 surface protein four days after addition of 4-OHT or EtOH vehicle to parental MCF10A and HKE-3 cells.

(**D**) Western blotting analysis of ER-KRAS^{G12V} type II pneumocytes treated with 4-OHT, MEK inhibitor or PI3K inhibitor in starvation medium for 24 h.

(**E**) qPCR analysis of *PD-L1* expression in H23 and H1792 cells 24 h after addition of MEK inhibitor or PI3K inhibitor or the combination. Mean ± SEM of three (H23) or two (H1792) independent experiments. **P<0.005, *P<0.05; unpaired, two-tailed Student's *t*-tests.

(**F**) qPCR analysis of *PD-L1* expression in H358 and H23 cells 24 h after addition of the ERK1/2 inhibitor SCH772984 (500 nM). Mean ± SD of biological duplicates. **P<0.01; unpaired, two-tailed Student's *t*-tests.

(**G**) qPCR analysis of *PD-L1* expression in H1792 cells treated with PMA for 3 h following a 30 min pre-treatment with DMSO or MEK inhibitor. Data represent the mean ± SEM of two independent experiments. ****P<0.0001; unpaired, two-tailed Student's *t*-test.

(**H**) Surface expression of PD-L1 was measured by flow cytometry. MFI values are adjusted for the isotype control in each condition. Mean ± SEM of biological duplicates.

(**I**) qPCR analysis of transcripts encoding antigen processing and presentation machinery in ER-KRAS^{G12V} type II pneumocytes simulated with 4-OHT for 24

h in starvation medium. Data represent the mean ± SEM of four independent experiments. ***P*<0.01; paired, two-tailed Student's *t*-test.
MFI, Mean Fluorescence Intensity. 4-OHT, 100 nM. IFN-γ, 20 ng/ml. MEK inhibitor GSK1120212, 25 nM. PI3K inhibitor GDC-0941, 500 nM. PMA, 200 nM.

Figure S2, relating to Figure 2. RAS Signalling Increases *PD-L1* mRNA Stability through AU-rich Elements in the 3'UTR

(**A**) Normalised luciferase signal from the indicated human CD274 promoter region reporter constructs in H358 cells treated for 6.5 h with medium only, PMA (200 nM) or IFN-γ (20 ng/ml). Numbering corresponds to the GRCh38 assembly. Data are representative of two independent experiments.
***P*<0.005, two-way ANOVA.
(**B**) Stability of murine *PD-L1* mRNA measured by qPCR after the addition of actinomycin D (5 μg/ml) and DMSO or PI3K inhibitor GDC-0941 (500 nM). KPB6 cells were pre-treated with DMSO or PI3K inhibitor for 30 min before actinomycin D addition. Data represent the mean ± SEM and are normalised to the 0 h time point when actinomycin D was added, and are representative of two independent experiments.
(**C**) Stability of murine *Tusc2* mRNA (left panel) and *Ptgs2* mRNA (right panel) measured by qPCR after the addition of actinomycin D (5 μg/ml) and DMSO or MEK inhibitor GSK1120212 (25 nM). KPB6 cells were pre-treated with DMSO or MEK inhibitor for 30 min before actinomycin D addition. Data represent the mean ± SEM and are normalised to the 0 h time point when actinomycin D was added.

Figure S3, relating to Figure 3. AU-rich element Binding Proteins TTP and KSRP are Negative Regulators of PD-L1 Expression

(**A-C**) qPCR analysis of knockdown efficiency 48 h after siRNA transfections, relative to siScrambled control. Data represent the mean ± SD of triplicates.

(**D**) qPCR analysis of *PD-L1* expression 24 h after transfection with the indicated constructs. Data represent the mean ± SEM of two independent experiments. ****$P<0.0001$; **$P<0.01$; unpaired, two-tailed Student's *t*-test.

(**E**) qPCR analysis of *PD-L1* expression in H23 cells 48 h after transfection with siRNAs targeting AU-rich binding proteins (AU-BPs), relative to siScrambled (siSc) control. Data represent the mean ± SEM of two independent experiments.

(**F**) qPCR analysis of knock-down efficiency in H23 cells 48 h after siRNA transfections, relative to siScrambled control. Data represent the mean ± SEM of two independent experiments.

(**G**) Western blotting analysis of TTP expression in H23, A427 and H358 cells 48 h after siRNA transfection with siRNA pools against TTP relative to siScrambled. Overexpression of Myc-TTP serves as a positive control for immunodetection.

(**H**) qPCR analysis of *PD-L1* and *TTP* expression in H23 and H358 cells 48 h after siRNA transfection with siRNA pools or single siRNAs against TTP relative to siScrambled. Data represent the mean ± SEM of biological duplicates.

Figure S4, relating to Figure 4. RAS Regulates *PD-L1* Expression through TTP

(**A**) qPCR analysis of *PD-L1* and *KSRP* expression in H358 cells following siRNA mediated knock-down of *KSRP* (24 h) followed by MEK inhibition (24 h) with GSK1120212 (25 nM). Data represent the mean ± SEM of two independent experiments. ****P<0.0001; ***P<0.001; **P<0.005; *P<0.05; n.s; not significant.

(**B**) qPCR analysis of *PD-L1* mRNA from RNA immunoprecipitates using IgG control or anti-TTP antibody, or anti-KSRP antibody, with lysate from KPB6 cells pre-treated with DMSO or MEK inhibitor GSK1120212 for 5.5 h (25 nM). Data represent the mean ± SD of biological triplicate IPs.

(**C**) qPCR analysis of *Gapdh* mRNA (control, lacking AU-rich elements) from RNA immunoprecipitates using IgG control or anti-TTP antibody, or anti-KSRP antibody, with lysate from KPB6 cells pre-treated with DMSO or MEK inhibitor GSK1120212 for 5.5 h (25 nM). Data represent the mean ± SD of biological triplicate IPs.

(**D**) qPCR analysis of *PD-L1* expression in H358 cells 24 after transfection with empty, wild-type KSRP or phospho-mutant KSRP^{S193A} constructs. Data represent the mean ± SEM of two independent experiments. ****P<0.0001; ***P<0.001; NS, not significant.

Unless otherwise stated, data were compared using unpaired, two-tailed Student's *t*-tests.

Figure S5, relating to Figure 5. RAS-ROS-p38 Signalling Controls TTP Activity

(**A**) MS/MS spectra for phosphopeptides STphSLVEGR (S52) and QSIphSFSGLPSGR (S178). -98 indicates the loss of H_3PO_4.

(**B**) Flow cytometry analysis of PD-L1 surface protein, and intracellular ROS measured by staining with H_2DCFDA, in MCF10A ER-HRASG12V cells treated with 4-OHT or vehicle ± NAC (10 mM) for 24 h. The same dataset is represented as a dot-plot and a histogram and data are representative of two independent experiments.

(**C**) Western blotting analysis of MCF10A cells harbouring an inducible version of the kinase domain of MEKK3 (ER-ΔMEKK3), 24 h after the addition of 4-OHT (100 nM) or vehicle.

(**D**) qPCR analysis of *PD-L1* mRNA expression 24 h after treatment with NAC (10 mM), reduced glutathione (1 mM) or MK2 inhibitor III (1 μM). Data represent the mean ± SEM of two independent experiments. ***P*< 0.01, ****P*<0.005, *****P*<0.001; two-tailed Student's *t*-tests comparing to DMSO control condition.

(**E**) Western blotting analysis of CT26 TTP KO cells harbouring doxycycline-inducible WT or phospho-mutant Myc-TTP constructs, treated with doxycycline or vehicle for 24 h. Arrow indicates Myc-TTP.

Figure S6, relating to Figure 6. RAS Pathway Activation is Associated with PD-L1 Upregulation in Human Lung Cancer

(**A**) Heat maps showing LUAD and COAD samples from the TCGA dataset clustered into RAS high or low pathway activity groups using RNA sequencing expression data and published RAS activity gene expression signatures (Loboda et al., 2010; Sweet-Cordero et al., 2005). *KRAS* mutation status (codons 12, 13 and 61) is shown for each sample.

(**B**) qPCR analysis of *PD-L1* and *IFNGR1* expression in ER-KRAS^{G12V} type II pneumocytes 24 h after treatment with vehicle, 4-OHT (100 nM), or 4-OHT with IFN-γ blocking antibody (10 μg/ml) or with ruxolitinib (500 nM). Mean ± SEM of two independent experiments. The panel on the right shows a qPCR analysis of *PD-L1* expression in ER-KRAS^{G12V} type II pneumocytes following a 30 h treatment with IFN-γ (20 ng/ml) and IFN-γ with IFN-γ blocking antibody (10 μg/ml) or with ruxolitinib (500 nM) to verify blocking of IFN-γ – IFGR1 signalling.

(**C**) *TTP* mRNA expression in human patient lung and colon normal tissue versus adenocarcinoma, from publically available datasets (Selamat et al., 2012; Skrzypczak et al., 2010). Wilcoxon signed-rank test.

(**D**) qPCR analysis of *PD-L1* and *TTP* expression in FACS purified CD45$^-$ CD31$^-$DAPI$^-$EpCAM$^+$ cells derived from lung tumours or matched normal adjacent lung tissue from *Kras*$^{LSL\text{-}G12D/+}$; *Trp53*$^{F/F}$ mice. Each point represents data from an individual mouse and is normalized to the matched normal lung tissue. ***P<0.0005; unpaired, two-tailed Student's *t*-tests.

(**E**) Flow cytometry analysis of PD-L1 expression on CD45-CD31-DAPI- cells derived from macroscopically dissected lung tumours or normal adjacent lung tissue from *Kras*$^{LSL\text{-}G12D/+}$; *Trp53*$^{F/F}$ mice. Each point represents data from an individual mouse and is normalized to the matched normal lung tissue. Data are pooled from two independent experiments. MFI; Mean Fluorescence Intensity. *P<0.05; unpaired, two-tailed Student's *t*-test.

Figure S7, relating to Figure 7. Restoration of Tumour Cell TTP Expression Enhances Anti-tumour Immunity

(**A**) Stability of murine *PD-L1* mRNA measured by qPCR analysis. CT26 TTP (tetON) cells were pretreated with doxycycline (Dox.; 1 μg/ml) or vehicle for 16 h and then MEK inhibitor (GSK1120212, trametinib; 25 nM) for an additional 30 min before actinomycin D (ActD; 10 μg/ml) was added. Data are normalized to time 0 h when ActD was added and represent the mean ± SEM of two independent experiments.

(**B**) Western blotting analysis of stable MC38 cell lines expressing Myc-tagged, mouse TTP under a tetracycline-inducible promoter (TTP tet-ON). Cells were treated with doxycycline (Dox., 0.1 μg/ml or 1 μg/ml) or vehicle in starvation medium for 24 h before analysis. Arrow indicates Myc-TTP.

(**C**) qPCR analysis of *PD-L1* expression from stable MC38 (TTP tet-ON) cell lines treated with doxycycline (Dox., 1 μg/ml) or vehicle in starvation medium for 40 h before analysis. Data represent the mean ± SEM of biological duplicates.

(**D**) Confluency was measured using IncuCyte for CT26 stable derivative cell lines treated with the indicated concentrations of doxycycline or vehicle at t = 0 h. Data represent the mean ± SD of biological triplicates and are representative of two independent experiments.

(**E**) Confluency was measured using IncuCyte for MC38 stable derivative cell lines treated with the indicated concentrations of doxycycline or vehicle at t = 0 h. Data represent the mean ± SD of biological triplicates.

(**F**) Representative histograms from flow cytometry analysis of PD-L1 surface expression in TTP (tetON) CT26 stable cells lines expressing endogenous PD-L1, PD-L1 + wild-type 3'UTR cDNA, or PD-L1 Δ3'UTR cDNA, after treatment with doxycycline (Dox., 1 μg/ml) or vehicle for 72 h. Data are representative of two independent experiments and also form part of Figure 7B.

(**G**) Tumour growth curves for the indicated CT26-derived cell lines shown in Figure S7C, subcutaneously transplanted into BALB/c mice (n = 5 WT 3'UTR + Dox and Δ3'UTR + H_2O; n = 4 WT 3'UTR + H_2O and Δ3'UTR + Dox; n = 3

empty + H_2O and empty + Dox). Vehicle or doxycycline (Dox., 50 mg/kg) was administered by oral gavage and commenced from day three after tumour cell injection. Mean ± SEM. ****P<0.0001, ***P<0.001, *P<0.05; two-way ANOVA.
(**H**) Representative histological analysis of CD3+ cells in subcutaneous tumours at the end-point from the experiment described in Figure 7C, and quantified in Figure 7G. Scale bar is 500 μm.
(**I**) Proposed molecular model. Oncogenic RAS activity leads to hyperphosphorylation, whereas PP2A activity promotes hypophosphorylation of TTP (Bourcier et al., 2011; Deleault et al., 2008; Essafi-Benkhadir et al., 2007; Hardle et al., 2015; Rahman et al., 2015; Sun et al., 2007), constituting a rapid switch controlling TTP activity. Low TTP expression and activity in tumour cells represents a permissive context for PD-L1 expression and immune evasion.

Table S1, relating to Figure 5 and Figure S5. TTP phosphopeptides.
Identified mouse TTP phosphopeptides from MS analyses pooled from two independent biological experiments. Identifications are 1 % FDR controlled. PEP indicates the probability that the identification is incorrect. Phosphosite assignment probabilities are indicated in parenthesis.

PEP	Score	Position	Modified sequence	Phospho (STY) Probabilities	Number of Phospho (STY)
0.01167	100	52	_STS(ph)LVEGR_	STS(1)LVEGR	1
1.41E-10	70	80	_PGPELS(ph)PSPT(ph)SPTATPTTSSR_	PGPELS(0.998)PS(0.006)PT(0.477)S(0.43)PT(0.068)AT(0.011)PT(0.002)T(0.002)S(0.002)S(0.003)R	2
1.41E-10	69	82	_PGPELSPS(ph)PTSPTATPTTSSR_	PGPELS(0.036)PS(0.911)PT(0.04)S(0.009)PT(0.002)AT(0.001)PTTSSR	1
1.07E-52	186	85	_PGPELSPSPTS(ph)PTATPTTSSR_	PGPELSPSPT(0.128)S(0.857)PT(0.013)ATPTTSSR	1
0.0404	74	105	_TYS(ph)ESGRCR_	TYS(1)ESGRCR	1
6.90E-08	130	178	_QSIS(ph)FSGLPSGR_	QSIS(1)FSGLPSGR	1
1.50E-22	96	189	_RSS(ph)PPPPGFS(ph)GPSLSSCSFSPSSSPPPPGDLPLSPSAFSAAPGTPVTR_	RS(0.17)S(0.767)PPPPGFS(0.195)GPS(0.146)LS(0.131)S(0.124)CS(0.111)FS(0.1)PS(0.09)S(0.085)S(0.081)PPPPGDLPLSPSAFSAAPGTPVTR	2
1.50E-22	96	196	_RSSPPPPGFS(ph)GPS(ph)LSSCSFSPSSSPPPPGDLPLSPSAFSAAPGTPVTR_	RS(0.051)S(0.25)PPPPGFS(0.367)GPS(0.173)LS(0.169)S(0.167)CS(0.166)FS(0.165)PS(0.165)S(0.164)S(0.164)PPPPGDLPLSPSAFSAAPGTPVTR	2
1.50E-22	96	199	_RSS(ph)PPPPGFS(ph)GPS(ph)LSSCSFSPSSSPPPGDLPLSPSAFSAAPGTPVTR_	RS(0.072)S(0.368)PPPPGFS(0.279)GPS(0.303)LS(0.3)S(0.297)CS(0.29)FS(0.282)PS(0.274)S(0.27)S(0.265)PPPPGDLPLSPSAFSAAPGTPVTR	2
9.68E-15	69	201	_RSSPPPPGFS(ph)GPS(ph)LSSCSFSPSSSPPPPGDLPLSPSAFSAAPGTPVTR_	RS(0.013)S(0.177)PPPPGFS(0.202)GPS(0.201)LS(0.201)S(0.201)CS(0.201)FS(0.201)PS(0.201)S(0.201)S(0.201)PPPPGDLPLSPSAFSAAPGTPVTR	2
9.68E-15	69	202	_RSSPPPPGFS(ph)GPS(ph)LSSCSFSPSSSPPPPGDLPLSPSAFSAAPGTPVTR_	RS(0.013)S(0.177)PPPPGFS(0.202)GPS(0.201)LS(0.201)S(0.201)CS(0.201)FS(0.201)PS(0.201)S(0.201)S(0.201)PPPPGDLPLSPSAFSAAPGTPVTR	2
9.68E-15	69	204	_RSSPPPPGFS(ph)GPS(ph)LSSCSFSPSSSPPPPGDLPLSPSAFSAAPGTPVTR_	RS(0.013)S(0.177)PPPPGFS(0.202)GPS(0.201)LS(0.201)S(0.201)CS(0.201)FS(0.201)PS(0.201)S(0.201)S(0.201)PPPPGDLPLSPSAFSAAPGTPVTR	2
9.68E-15	69	206	_RSSPPPPGFS(ph)GPS(ph)LSSCSFSPSSSPPPPGDLPLSPSAFSAAPGTPVTR_	RS(0.013)S(0.177)PPPPGFS(0.202)GPS(0.201)LS(0.201)S(0.201)CS(0.201)FS(0.201)PS(0.201)S(0.201)S(0.201)PPPPGDLPLSPSAFSAAPGTPVTR	2
9.68E-15	69	208	_RSSPPPPGFS(ph)GPS(ph)LSSCSFSPSSSPPPPGDLPLSPSAFSAAPGTPVTR_	RS(0.013)S(0.177)PPPPGFS(0.202)GPS(0.201)LS(0.201)S(0.201)CS(0.201)FS(0.201)PS(0.201)S(0.201)S(0.201)PPPPGDLPLSPSAFSAAPGTPVTR	2
9.68E-15	69	209	_RSSPPPPGFS(ph)GPS(ph)LSSCSFSPSSSPPPPGDLPLSPSAFSAAPGTPVTR_	RS(0.013)S(0.177)PPPPGFS(0.202)GPS(0.201)LS(0.201)S(0.201)CS(0.201)FS(0.201)PS(0.201)S(0.201)S(0.201)PPPPGDLPLSPSAFSAAPGTPVTR	2
9.68E-15	69	210	_RSSPPPPGFS(ph)GPS(ph)LSSCSFSPSSSPPPPGDLPLSPSAFSAAPGTPVTR_	RS(0.013)S(0.177)PPPPGFS(0.202)GPS(0.201)LS(0.201)S(0.201)CS(0.201)FS(0.201)PS(0.201)S(0.201)S(0.201)PPPPGDLPLSPSAFSAAPGTPVTR	2
0.00722	63	248	_S(ph)TTPSTIWGPLGGLAR_	S(0.333)T(0.333)T(0.333)PSTIWGPLGGLAR	1
0.00722	63	249	_S(ph)TTPSTIWGPLGGLAR_	S(0.333)T(0.333)T(0.333)PSTIWGPLGGLAR	1
1.93E-20	158	250	_STT(ph)PSTIWGPLGGLAR_	ST(0.003)T(0.997)PSTIWGPLGGLAR	1
6.07E-19	89	264	_S(ph)PSAHSLGSDPDDYASSGSSLGGSDSPVFEAGVFGPPQTPAPPR_	S(0.446)PS(0.412)AHS(0.087)LGS(0.022)DPDDY(0.004)AS(0.005)S(0.005)GS(0.005)S(0.005)LGGS(0.005)DS(0.005)PVFEAGVFGPPQTPAPPR	1
6.07E-19	89	266	_S(ph)PSAHSLGSDPDDYASSGSSLGGSDSPVFEAGVFGPPQTPAPPR_	S(0.41)PS(0.41)AHS(0.165)LGS(0.006)DPDDY(0.001)AS(0.001)S(0.001)GS(0.001)S(0.001)LGGS(0.001)DS(0.001)PVFEAGVFGPPQTPAPPR	1
5.37E-14	83	269	_SPSAHS(ph)LGSDPDDYASSGSSLGGSDSPVFEAGVFGPPQTPAPPR_	S(0.272)PS(0.272)AHS(0.447)LGS(0.004)DPDDY(0.001)AS(0.001)S(0.001)GS(0.001)S(0.001)LGGS(0.001)DS(0.001)PVFEAGVFGPPQTPAPPR	1
1.50E-07	59	272	_SPSAHSLGS(ph)DPDDYASSGSSLGGSDSPVFEAGVFGPPQTPAPPR_	S(0.019)PS(0.019)AHS(0.078)LGS(0.343)DPDDY(0.073)AS(0.078)S(0.078)GS(0.078)S(0.078)LGGS(0.078)DS(0.078)PVFEAGVFGPPQTPAPPR	1
0.0015	41	279	_SPSAHSLGS(ph)DPDDYASSGSSLGGSDSPVFEAGVFGPPQTPAPPR_	S(0.044)PS(0.044)AHS(0.044)LGS(0.109)DPDDY(0.103)AS(0.109)S(0.109)GS(0.109)S(0.109)LGGS(0.109)DS(0.109)PVFEAGVFGPPQTPAPPR	1
0.0015	41	280	_SPSAHSLGS(ph)DPDDYASSGSSLGGSDSPVFEAGVFGPPQTPAPPR_	S(0.044)PS(0.044)AHS(0.044)LGS(0.109)DPDDY(0.103)AS(0.109)S(0.109)GS(0.109)S(0.109)LGGS(0.109)DS(0.109)PVFEAGVFGPPQTPAPPR	1
0.0015	41	282	_SPSAHSLGS(ph)DPDDYASSGSSLGGSDSPVFEAGVFGPPQTPAPPR_	S(0.044)PS(0.044)AHS(0.044)LGS(0.109)DPDDY(0.103)AS(0.109)S(0.109)GS(0.109)S(0.109)LGGS(0.109)DS(0.109)PVFEAGVFGPPQTPAPPR	1
0.0015	41	283	_SPSAHSLGS(ph)DPDDYASSGSSLGGSDSPVFEAGVFGPPQTPAPPR_	S(0.044)PS(0.044)AHS(0.044)LGS(0.109)DPDDY(0.103)AS(0.109)S(0.109)GS(0.109)S(0.109)LGGS(0.109)DS(0.109)PVFEAGVFGPPQTPAPPR	1
0.0015	41	287	_SPSAHSLGS(ph)DPDDYASSGSSLGGSDSPVFEAGVFGPPQTPAPPR_	S(0.044)PS(0.044)AHS(0.044)LGS(0.109)DPDDY(0.103)AS(0.109)S(0.109)GS(0.109)S(0.109)LGGS(0.109)DS(0.109)PVFEAGVFGPPQTPAPPR	1
0.0015	41	289	_SPSAHSLGS(ph)DPDDYASSGSSLGGSDSPVFEAGVFGPPQTPAPPR_	S(0.044)PS(0.044)AHS(0.044)LGS(0.109)DPDDY(0.103)AS(0.109)S(0.109)GS(0.109)S(0.109)LGGS(0.109)DS(0.109)PVFEAGVFGPPQTPAPPR	1

Table S2, relating to STAR Methods, Method Details. Cell lines and growth conditions.

Cell line	Source	Normal medium	Starvation medium
H358	ATCC	RPMI + 10 % FCS	N/A
A427	CRUK Cell Services	RPMI + 10 % FCS	N/A
H1792	ATCC	RPMI + 10 % FCS	N/A
KPB6	Sergio Quezada Laboratory	DMEM + 10 % FCS	N/A
Type II pneumocytes	Olivier Pardo, Michael Seckl (Imperial College, London) and (Molina-Arcas et al., 2013a)	DCCM-1 + 10 % FCS	+ 0.5 % FCS for qPCR and FACS + 0 % FCS for mRNA half-life analysis
SW837	CRUK Cell Services	DMEM + 10 % FCS	N/A
H23	CRUK Cell Services	RPMI + 10 % FCS	N/A
293FT	CRUK Cell Services	DMEM + 10 % FCS	N/A
TTP KO and TTP WT MEFs	Perry Blackshear Laboratory	DMEM + 10 % FCS	+ 0.5 % FCS
MCF10A	(Molina-Arcas et al., 2013a)	F12:DMEM mix (1:1) and 5 % horse serum, 20 ng/ml EGF, 10 μg/ml insulin, 100 ng/ml cholera toxin, 0.5 μg/ml hydrocortisone	+ 5 % horse serum
CT26	CRUK Cell Services	RPMI + 10 % FCS	N/A
A549	CRUK Cell Services	DMEM + 10 % FCS	N/A
MC38	George Kassiotis Laboratory	RPMI + 10 % FCS	+ 0.5 % FCS

N/A, not applicable.

Figure S1

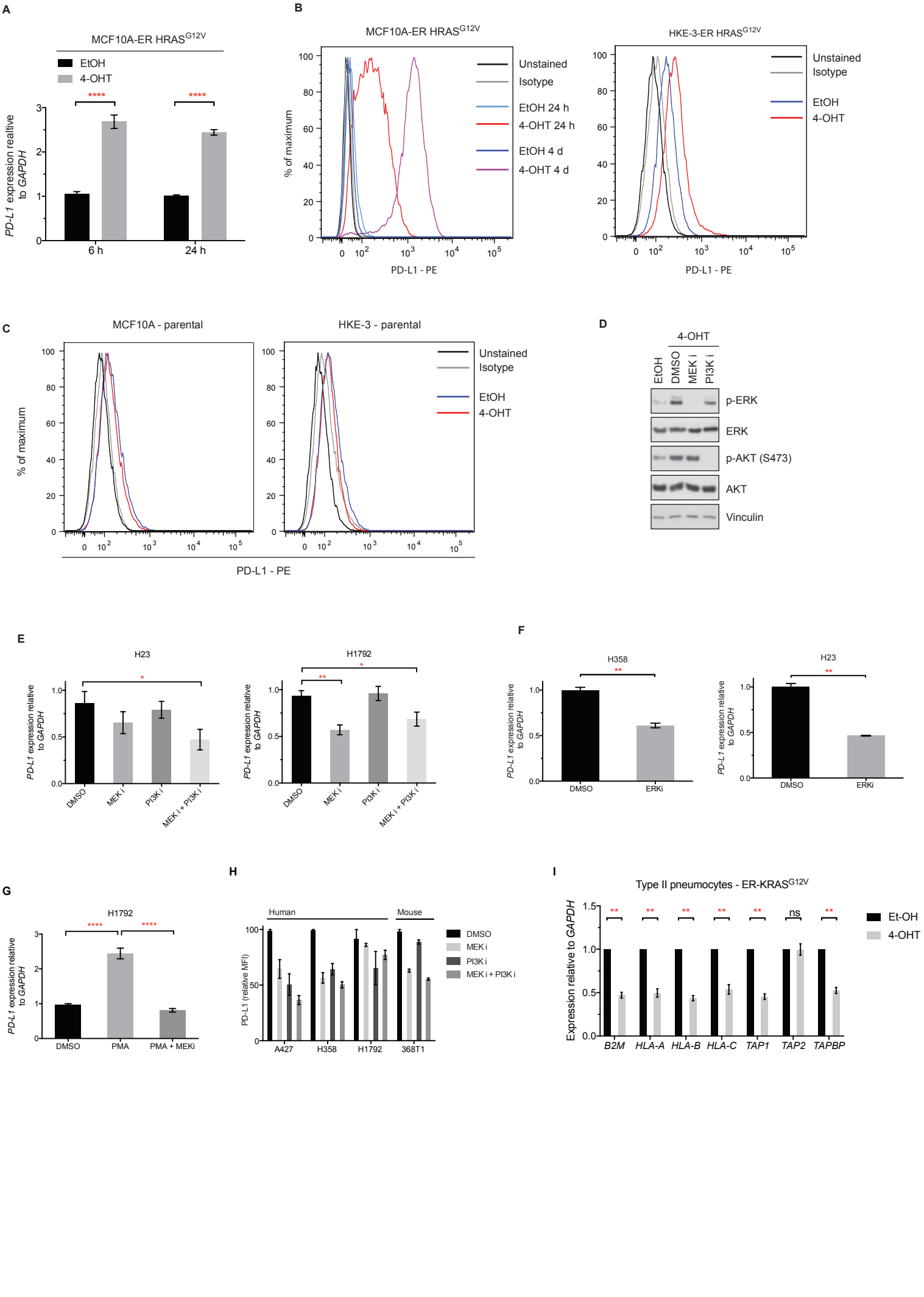
A
MCF10A-ER HRAS^{G12V}
EtOH
4-OHT
****
****
PD-L1 expression realtive to GAPDH
6 h
24 h
B
MCF10A-ER HRAS^{G12V}
% of maximum
Unstained
Isotype
EtOH 24 h
4-OHT 24 h
EtOH 4 d
4-OHT 4 d
PD-L1 - PE
HKE-3-ER HRAS^{G12V}
Unstained
Isotype
EtOH
4-OHT
PD-L1 - PE
C
MCF10A - parental
HKE-3 - parental
% of maximum
Unstained
Isotype
EtOH
4-OHT
PD-L1 - PE
D
4-OHT
EtOH
DMSO
MEK i
PI3K i
p-ERK
ERK
p-AKT (S473)
AKT
Vinculin
E
H23
H1792
PD-L1 expression relative to GAPDH
DMSO
MEK i
PI3K i
MEK i + PI3K i
F
H358
H23
PD-L1 expression relative to GAPDH
DMSO
ERKi
G
H1792
PD-L1 expression relative to GAPDH
DMSO
PMA
PMA + MEKi
H
Human
Mouse
PD-L1 (relative MFI)
DMSO
MEK i
PI3K i
MEK i + PI3K i
A427
H358
H1792
368T1
I
Type II pneumocytes - ER-KRAS^{G12V}
Expression relative to GAPDH
ns
Et-OH
4-OHT
B2M
HLA-A
HLA-B
HLA-C
TAP1
TAP2
TAPBP

Figure S2

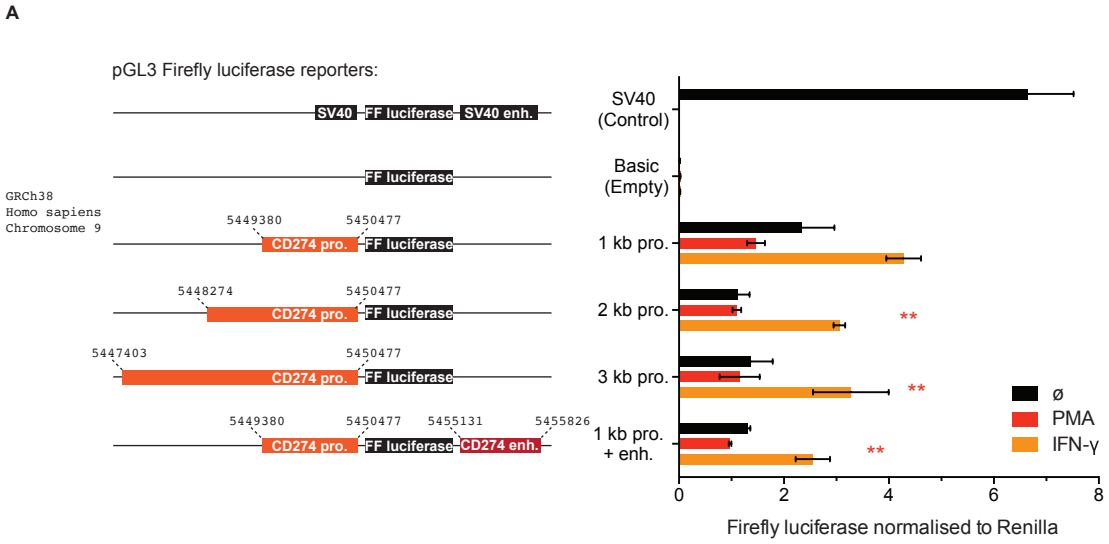
A
pGL3 Firefly luciferase reporters:
SV40
FF luciferase
SV40 enh.
FF luciferase
GRCh38
Homo sapiens
Chromosome 9
5449380
5450477
CD274 pro.
FF luciferase
5448274
5450477
CD274 pro.
FF luciferase
5447403
5450477
CD274 pro.
FF luciferase
5449380
5450477
5455131
5455826
CD274 pro.
FF luciferase
CD274 enh.
SV40 (Control)
Basic (Empty)
1 kb pro.
2 kb pro.
3 kb pro.
1 kb pro. + enh.
**
**
**
ø
PMA
IFN-γ
0
2
4
6
8
Firefly luciferase normalised to Renilla

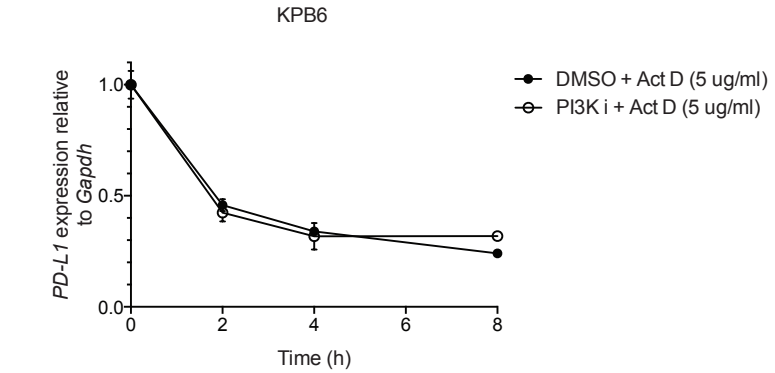
B
KPB6
PD-L1 expression relative to Gapdh
1.0
0.5
0.0
0
2
4
6
8
Time (h)
DMSO + Act D (5 ug/ml)
PI3K i + Act D (5 ug/ml)

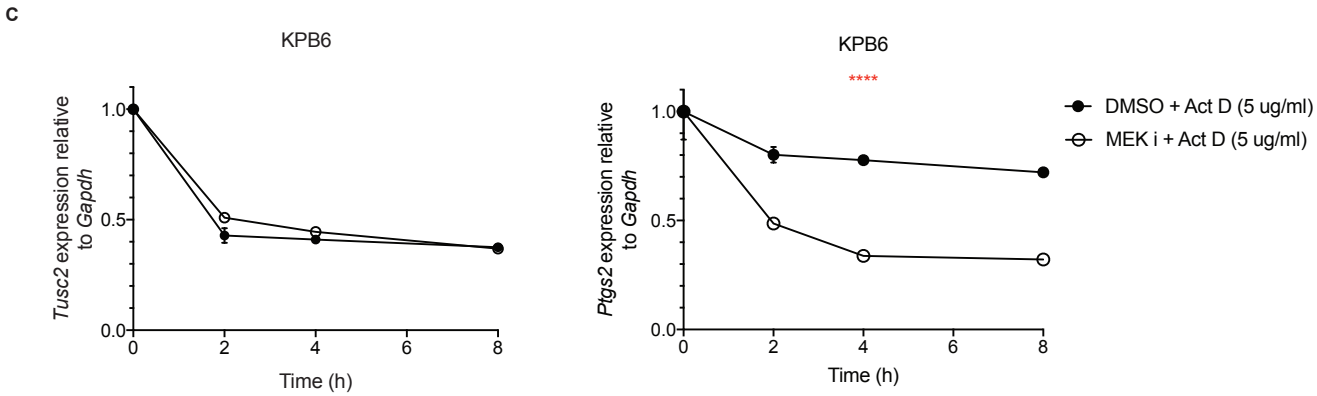
C
KPB6
Tusc2 expression relative to Gapdh
1.0
0.5
0.0
0
2
4
6
8
Time (h)
KPB6
****
Ptgs2 expression relative to Gapdh
1.0
0.5
0.0
0
2
4
6
8
Time (h)
DMSO + Act D (5 ug/ml)
MEK i + Act D (5 ug/ml)

Figure S3

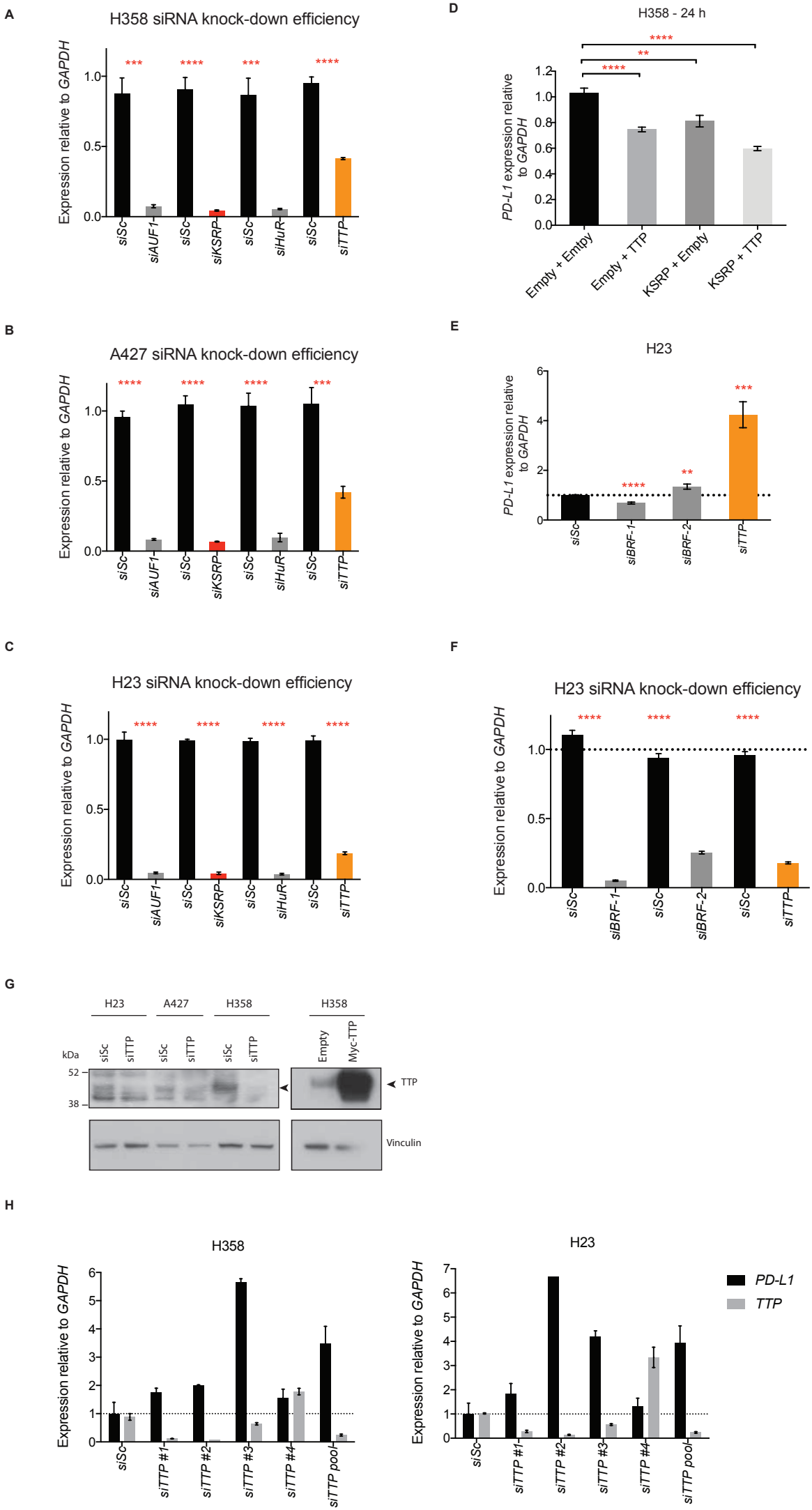
A
H358 siRNA knock-down efficiency
Expression relative to GAPDH
siSc
siAUF1
siKSRP
siHuR
siTTP
B
A427 siRNA knock-down efficiency
C
H23 siRNA knock-down efficiency
D
H358 - 24 h
PD-L1 expression relative to GAPDH
Empty + Emtpy
Empty + TTP
KSRP + Empty
KSRP + TTP
E
H23
siBRF-1
siBRF-2
F
G
H23
A427
H358
Empty
Myc-TTP
kDa
52
38
TTP
Vinculin
H
PD-L1
TTP
siTTP #1
siTTP #2
siTTP #3
siTTP #4
siTTP pool

Figure S4

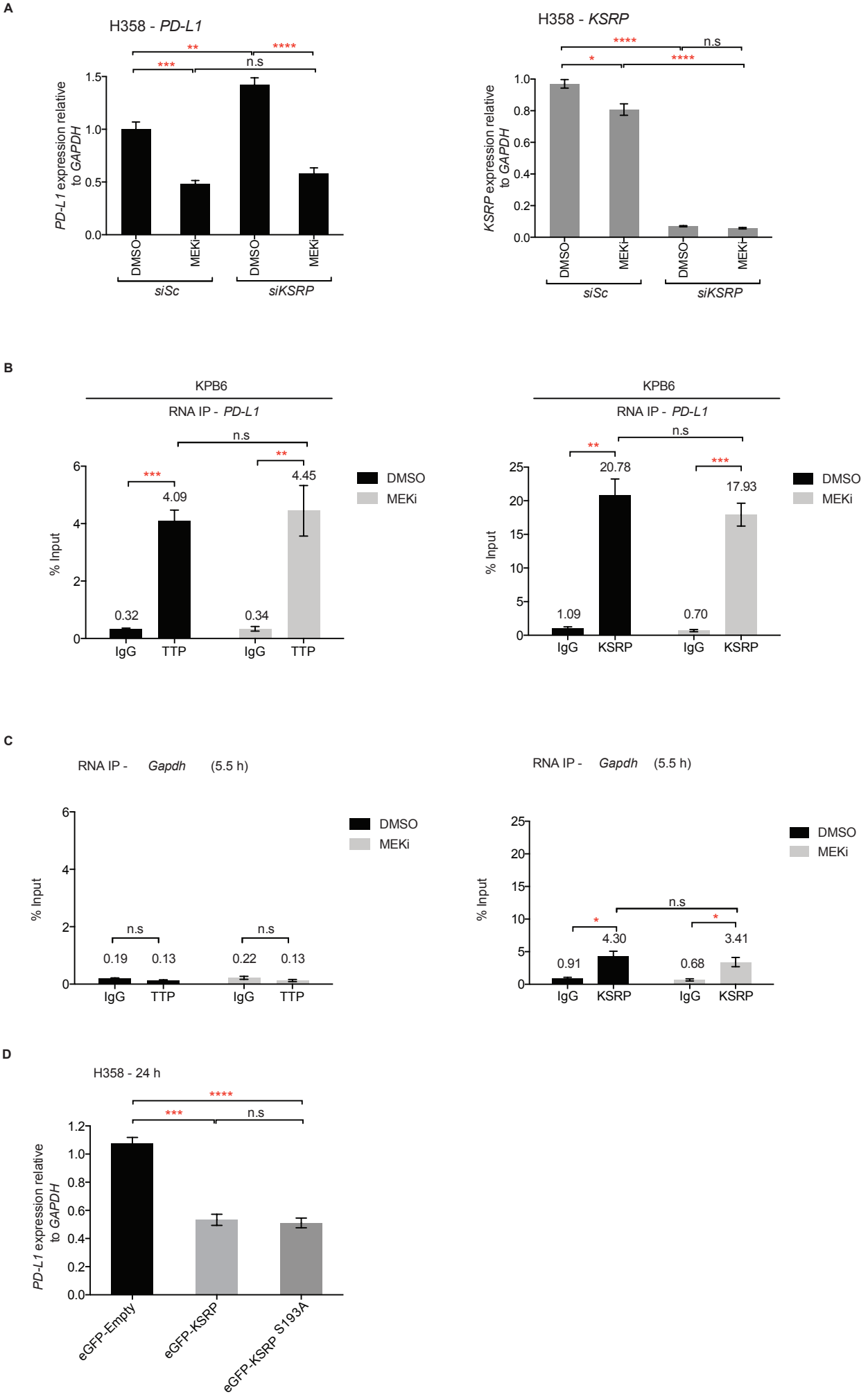
A
H358 - PD-L1
PD-L1 expression relative to GAPDH
DMSO
MEKi
siSc
siKSRP
H358 - KSRP
KSRP expression relative to GAPDH
B
KPB6
RNA IP - PD-L1
% Input
IgG
TTP
KSRP
C
RNA IP - Gapdh (5.5 h)
D
H358 - 24 h
eGFP-Empty
eGFP-KSRP
eGFP-KSRP S193A

Figure S5

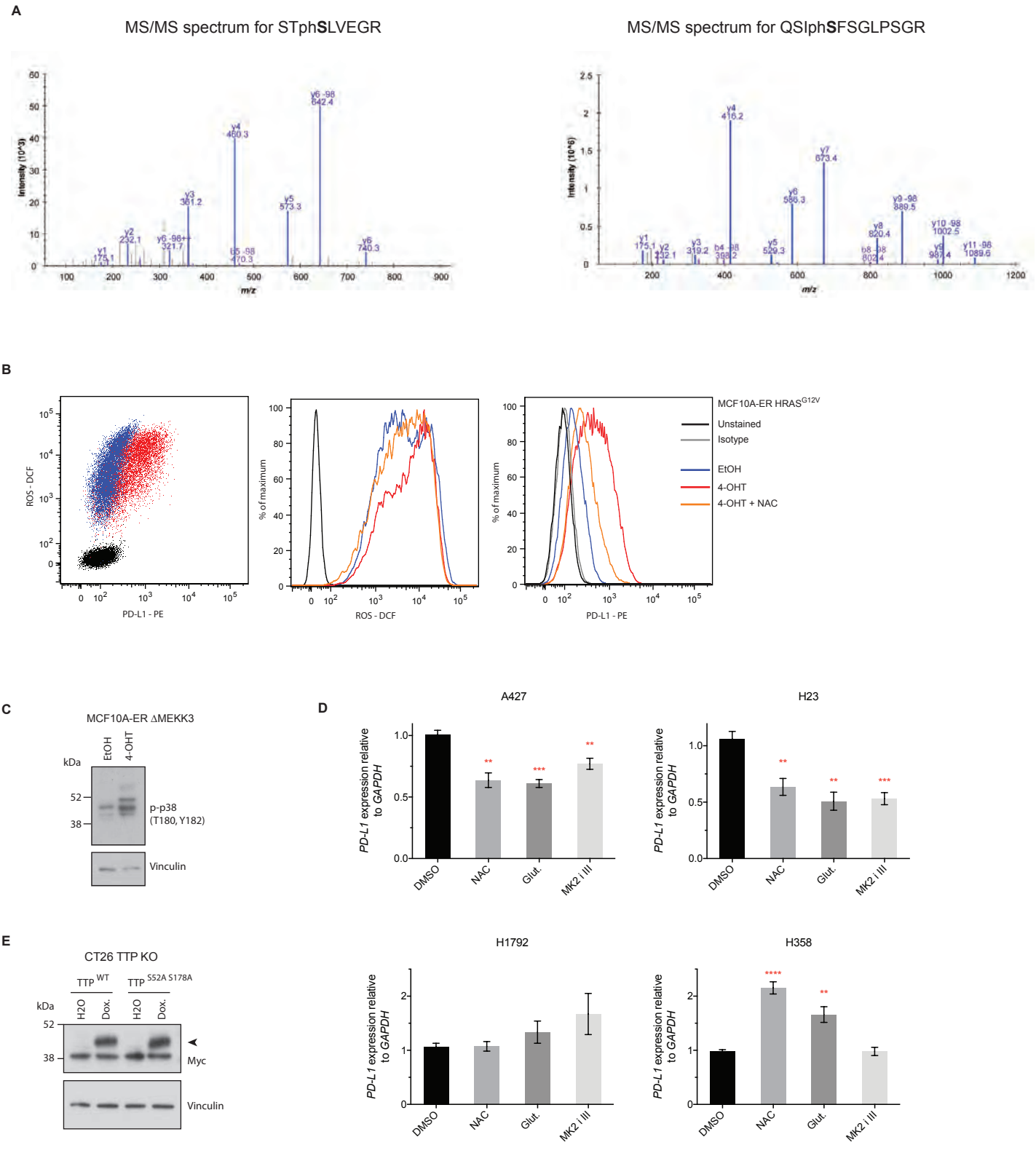
A
MS/MS spectrum for STph**S**LVEGR
MS/MS spectrum for QSIph**S**FSGLPSGR
B
ROS - DCF
PD-L1 - PE
% of maximum
ROS - DCF
% of maximum
PD-L1 - PE
MCF10A-ER HRAS^{G12V}
Unstained
Isotype
EtOH
4-OHT
4-OHT + NAC
C
MCF10A-ER ΔMEKK3
EtOH
4-OHT
kDa
52
38
p-p38
(T180, Y182)
Vinculin
D
A427
H23
PD-L1 expression relative to GAPDH
DMSO
NAC
Glut.
MK2 i III
E
CT26 TTP KO
TTP WT
TTP S52A S178A
kDa
H2O
Dox.
H2O
Dox.
52
38
Myc
Vinculin
H1792
H358
PD-L1 expression relative to GAPDH
DMSO
NAC
Glut.
MK2 i III

Figure S6

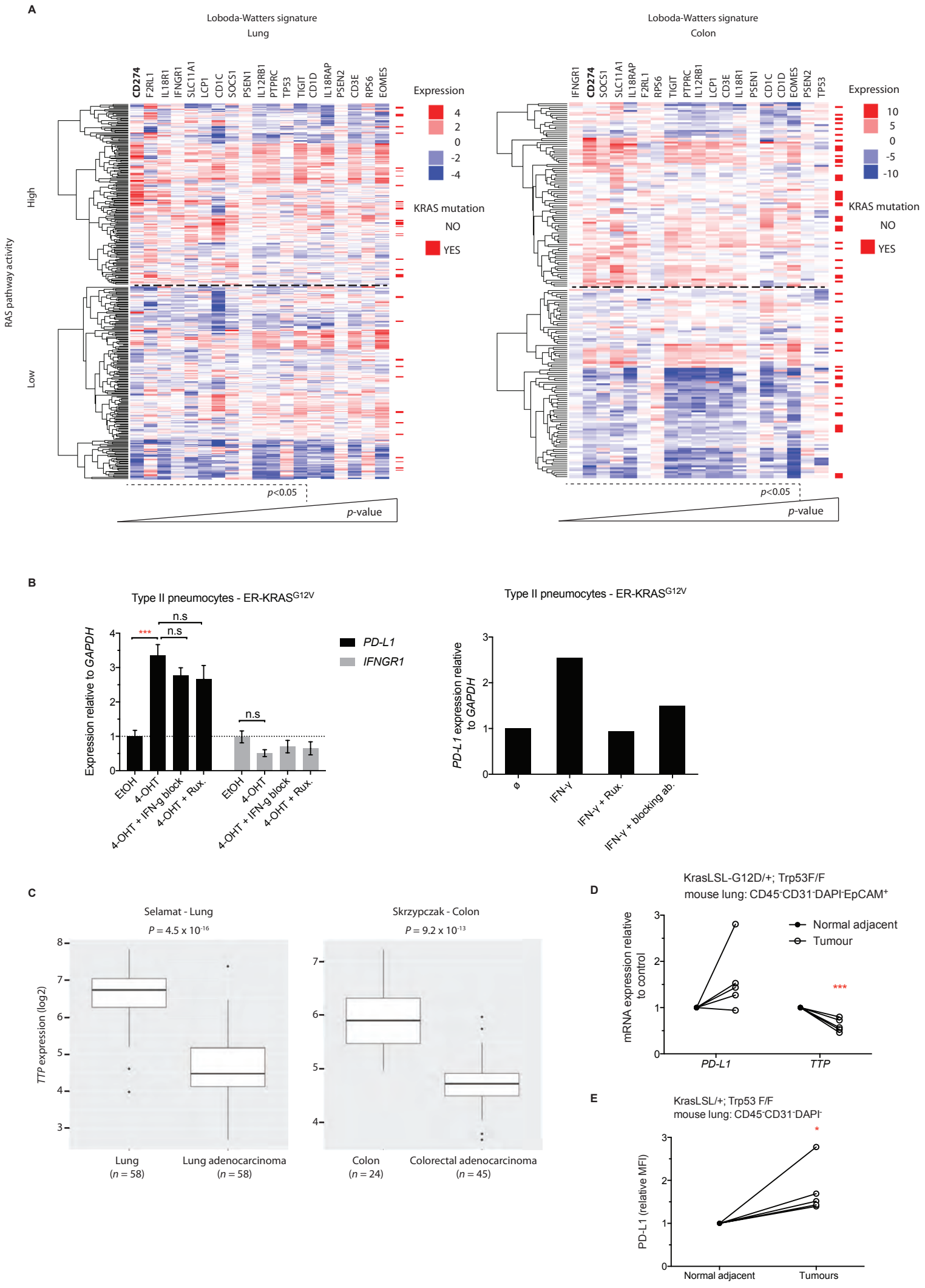
A
Loboda-Watters signature
Lung
CD274
F2RL1
IL18R1
IFNGR1
SLC11A1
LCP1
CD1C
SOCS1
PSEN1
IL12RB1
PTPRC
TP53
TIGIT
CD1D
IL18RAP
PSEN2
CD3E
RPS6
EOMES
Expression
4
2
0
-2
-4
KRAS mutation
NO
YES
High
Low
RAS pathway activity
p<0.05
p-value
Loboda-Watters signature
Colon
IFNGR1
CD274
SOCS1
SLC11A1
IL18RAP
F2RL1
RPS6
TIGIT
PTPRC
IL12RB1
LCP1
CD3E
IL18R1
PSEN1
CD1C
CD1D
EOMES
PSEN2
TP53
Expression
10
5
0
-5
-10
KRAS mutation
NO
YES
p<0.05
p-value
B
Type II pneumocytes - ER-KRASG12V
Expression relative to GAPDH
n.s
n.s
***
n.s
PD-L1
IFNGR1
EtOH
4-OHT
4-OHT + IFN-g block
4-OHT + Rux.
EtOH
4-OHT
4-OHT + IFN-g block
4-OHT + Rux.
Type II pneumocytes - ER-KRASG12V
PD-L1 expression relative to GAPDH
ø
IFN-γ
IFN-γ + Rux.
IFN-γ + blocking ab.
C
Selamat - Lung
P = 4.5 x 10-16
TTP expression (log2)
Lung (n = 58)
Lung adenocarcinoma (n = 58)
Skrzypczak - Colon
P = 9.2 x 10-13
Colon (n = 24)
Colorectal adenocarcinoma (n = 45)
D
KrasLSL-G12D/+; Trp53F/F
mouse lung: CD45-CD31-DAPI-EpCAM+
mRNA expression relative to control
Normal adjacent
Tumour
***
PD-L1
TTP
E
KrasLSL/+; Trp53 F/F
mouse lung: CD45-CD31-DAPI-
PD-L1 (relative MFI)
*
Normal adjacent
Tumours

Figure S7

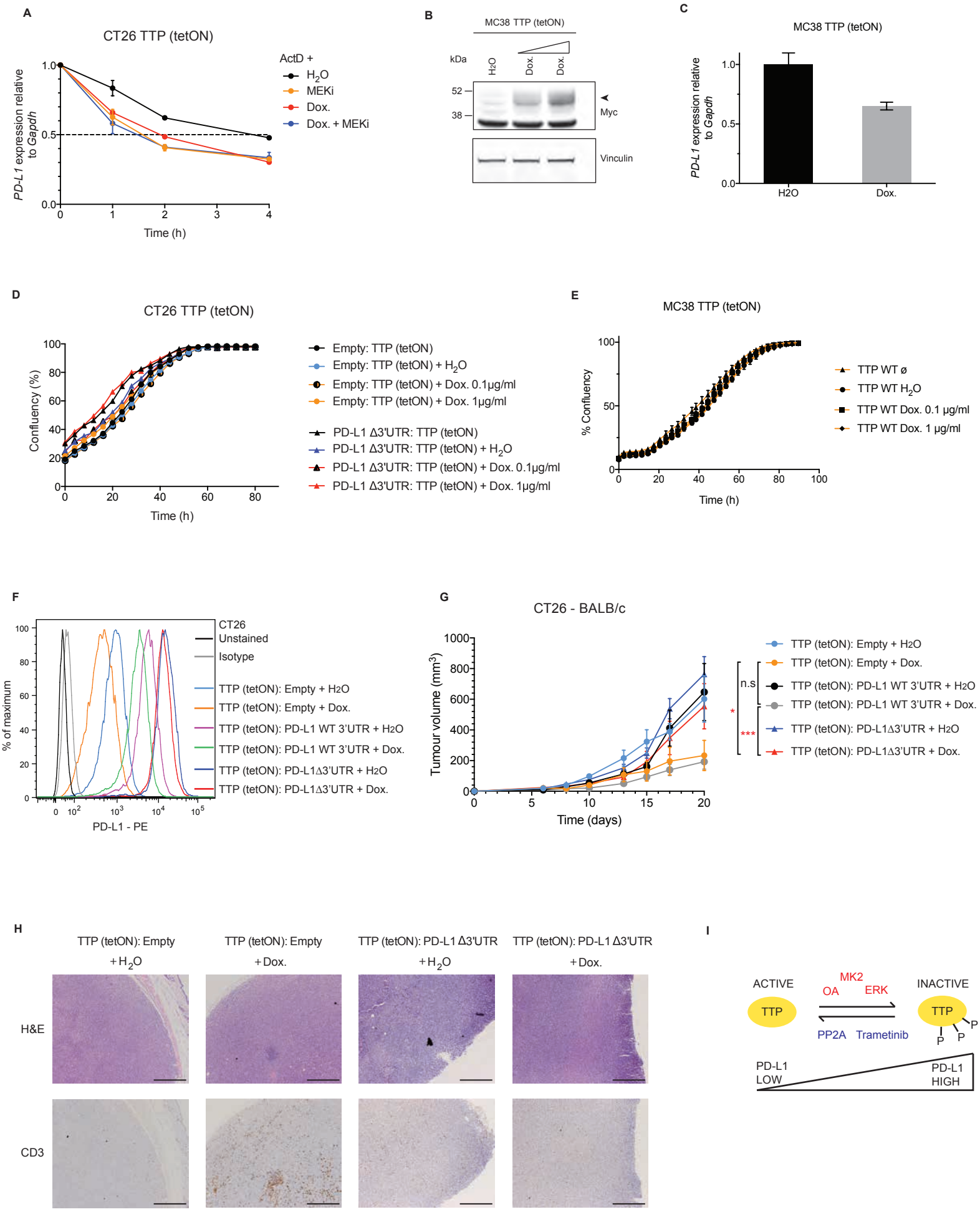
A
CT26 TTP (tetON)
PD-L1 expression relative to Gapdh
Time (h)
ActD +
H2O
MEKi
Dox.
Dox. + MEKi
B
MC38 TTP (tetON)
kDa
H2O
Dox.
Dox.
52
38
Myc
Vinculin
C
MC38 TTP (tetON)
PD-L1 expression relative to Gapdh
H2O
Dox.
D
CT26 TTP (tetON)
Confluency (%)
Time (h)
Empty: TTP (tetON)
Empty: TTP (tetON) + H2O
Empty: TTP (tetON) + Dox. 0.1µg/ml
Empty: TTP (tetON) + Dox. 1µg/ml
PD-L1 Δ3'UTR: TTP (tetON)
PD-L1 Δ3'UTR: TTP (tetON) + H2O
PD-L1 Δ3'UTR: TTP (tetON) + Dox. 0.1µg/ml
PD-L1 Δ3'UTR: TTP (tetON) + Dox. 1µg/ml
E
MC38 TTP (tetON)
% Confluency
Time (h)
TTP WT ø
TTP WT H2O
TTP WT Dox. 0.1 µg/ml
TTP WT Dox. 1 µg/ml
F
% of maximum
PD-L1 - PE
CT26
Unstained
Isotype
TTP (tetON): Empty + H2O
TTP (tetON): Empty + Dox.
TTP (tetON): PD-L1 WT 3'UTR + H2O
TTP (tetON): PD-L1 WT 3'UTR + Dox.
TTP (tetON): PD-L1Δ3'UTR + H2O
TTP (tetON): PD-L1Δ3'UTR + Dox.
G
CT26 - BALB/c
Tumour volume (mm3)
Time (days)
TTP (tetON): Empty + H2O
TTP (tetON): Empty + Dox.
TTP (tetON): PD-L1 WT 3'UTR + H2O
TTP (tetON): PD-L1 WT 3'UTR + Dox.
TTP (tetON): PD-L1Δ3'UTR + H2O
TTP (tetON): PD-L1Δ3'UTR + Dox.
n.s
*
***
H
TTP (tetON): Empty + H2O
TTP (tetON): Empty + Dox.
TTP (tetON): PD-L1 Δ3'UTR + H2O
TTP (tetON): PD-L1 Δ3'UTR + Dox.
H&E
CD3
I
ACTIVE
TTP
MK2
OA
ERK
PP2A
Trametinib
INACTIVE
TTP
P
P
P
PD-L1 LOW
PD-L1 HIGH